A STRAIN RELIEF MODEL FOR THE $In_xGa_{1-x}As/GaAs$ HETEROEPITAXIAL SYSTEM AND ITS APPLICATION TOWARD THE GROWTH OF LOW-DISLOCATION DENSITY LARGE In CONTENT $In_xGa_{1-x}As$

By

VISWANATH KRISHNAMOORTHY

A DISSERTATION PRESENTED TO THE GRADUATE SCHOOL
OF THE UNIVERSITY OF FLORIDA IN PARTIAL FULFILLMENT
OF THE REQUIREMENTS FOR THE DEGREE OF
DOCTOR OF PHILOSOPHY

UNIVERSITY OF FLORIDA

1992

ACKNOWLEDGEMENTS

The author wishes to thank his supervisory committee chairman Dr. R.M. Park for his guidance and support during the research and the writing of this dissertation. The advice and support of the other members of this committee, namely, Dr. K.S. Jones, Dr. P.H. Holloway, Dr. R.T. DeHoff and Dr. S.S. Li, are also gratefully acknowledged. Special gratitude is due to Dr. Y.W. Lin and Bruce Liu for their tireless and impeccable work in growing a seemingly endless tirade of heterostructures. The author also wishes to thank D. Venables and D.T. Hoelzer for their intellectual and moral support and C. Rouleau, M.J. Troffer, L. Calhoun and P. Ribas for putting up with his never ending monologues.

The author also wishes to thank his family for their support and understanding during these trying times and his friends for irking his competitive spirit with rude remarks about his intellectual capacity.

TABLE OF CONTENTS

page

ACKNOWLEDGEMENTS.....ii

ABSTRACT.....

CHAPTERS

1 INTRODUCTION.....1

1.1 Motivation and Objectives.....1
1.2 Background.....3
1.2.1 Critical Thickness in Lattice-Mismatched Systems.....4
1.2.2 Strain Relief Mechanisms.....9
1.2.3 Dislocation Evolution in the $In_xGa_{1-x}As$/GaAs Material System..... 14
1.2.4 Common Buffer Structures Used to Block Dislocations.....19
1.2.5 Summary.....23
1.3 Scope of the Present Work.....23

2 GROWTH AND CHARACTERIZATION TECHNIQUES.....25

2.1 Molecular Beam Epitaxy.....25
2.2 Characterization Techniques.....31
2.2.1 Transmission Electron Microscopy.....31
2.2.1.1 Cross-sectional TEM specimen preparation technique.....32
2.2.1.2 Plan-view TEM specimen preparation technique.....33
2.2.2 Etch Pit Technique.....33
2.2.3 Electron Microprobe Analysis.....34
2.2.4 High Resolution X-Ray Diffraction.....34
2.2.4.1 Phillips high resolution x-ray diffractometer.....35
2.2.4.2 Optimization procedures.....42
2.2.4.3 Strain analysis using HRXRD.....46

3 STRAIN RELIEF IN $In_xGa_{1-x}As/GaAs$ SINGLE HETEROSTRUCTURES....50

3.1 Introduction....50
3.2 XTEM analysis of $In_xGa_{1-x}As/GaAs$ Single Layer Structures....51
3.3 Discussion of Results....58
3.4 A Force Balance Mechanism for Dislocation Evolution....64
3.5 Summary....70

4 STRAIN RELIEF IN $In_xGa_{1-x}As$-BASED STRAIN LAYER SUPERLATTICE SYSTEMS....71

4.1 Introduction....71
4.2 Single Strained Layer Superlattice Buffer Structures..71
4.3 Design and Analysis of Multistage Strain Relief Systems Containing Strained Layer Superlattices....75
4.4 Summary and Conclusions....90

5 STRAIN RELIEF IN STACKED $In_xGa_{1-x}As$ MULTILAYER SYSTEMS NOT INVOLVING STRAINED LAYER SUPERLATTICES....91

5.1 Introduction....91
5.2 Extent of Residual Strain in Single $In_xGa_{1-x}As/GaAs$ Heterostructures....92
5.3 Strain Relaxation in Stacked $In_xGa_{1-x}As$ Multilayer Structures....102

6 CONCLUSIONS AND RECOMMENDATIONS....120

REFERENCES....123

BIOGRAPHICAL SKETCH....127

Abstract of Dissertation Presented to the Graduate School
of the University of Florida in Partial Fulfillment of the
Requirements for the Degree of Doctor of Philosophy

STRAIN RELIEF MODEL FOR THE $In_xGa_{1-x}As$/GaAs SYSTEM AND ITS APPLICATION TOWARD THE GROWTH OF LOW DISLOCATION DENSITY $In_xGa_{1-x}As$

By

Viswanath Krishnamoorthy

August 1992

Chairman: Dr. Robert. M. Park
Major Department: Materials Science and Engineering

Strain relaxation occurring in the $In_xGa_{1-x}As$/GaAs heteroepitaxial system as a function of $In_xGa_{1-x}As$ composition was studied extensively using transmission electron microscopy, to observe dislocation evolution, and high resolution x-ray diffraction, to determine the extent of strain relaxation. Both single $In_xGa_{1-x}As$/GaAs heterostructures and stacked $In_xGa_{1-x}As$ multiple layer systems were analysed.

In the case of stacked multiple layer $In_xGa_{1-x}As$/GaAs systems, it was discovered that low-dislocation density $In_xGa_{1-x}As$ top layers (layers on top of the stacked structures) can be grown provided that the compositional difference between two adjacent $In_xGa_{1-x}As$ layers in the stack is maintained below a determined critical compositional difference of $\Delta x \approx 0.18$, taking partial lattice-relaxation properly into account. For this case it was determined that dislocation evolution is confined to the GaAs substrate and the $In_xGa_{1-x}As$ layers underlying

the top $In_xGa_{1-x}As$ layer in the stack, the top $In_xGa_{1-x}As$ layer being essentially dislocation-free. This phenomenon is attributed to a monotonic increase in the yield strength of $In_xGa_{1-x}As$ at the appropriate growth temperatures with increasing values of x. Such behaviour appears to persist up to an $In_xGa_{1-x}As$ composition of approximately x=0.5, whereupon a further increase in composition (increase in x value) results in dislocation evolution in the top layer of the stack. It is postulated that the yield strength of $In_xGa_{1-x}As$ decreases at elevated temperatures (growth temperatures) with increasing values of x beyond x=0.5.

It was determined that extremely low-dislocation density $In_xGa_{1-x}As$ material can be grown on GaAs using the stacked structure approach as evidenced by etch pit analysis. For example, dislocation densities of $1\text{-}2x10^3/cm^2$ and $5\text{-}6x10^3/cm^2$ were recorded from $In_{0.35}Ga_{0.65}As$ and $In_{0.48}Ga_{0.52}As$ top layers, respectively. Such $In_xGa_{1-x}As$ alloys would be potentially suitable for the fabrication of photonic devices operating at 1.3μm (x=0.35) and 1.55μm (x=0.48).

CHAPTER 1
INTRODUCTION

1.1 Motivation and Objectives

The incorporation of semiconductor heterostructures into electronic and photonic devices has in recent years led to dramatic improvements in device operating characteristics. For instance, heteroemitter bipolar transistors display higher current gain than conventional homojunction bipolar transistors, modulation-doped field-effect transistors or high-electron mobility transistors (HEMTs) operate at higher speeds than do conventional field-effect transistors and double-heterostructure diode lasers have greatly reduced threshold current densities compared to their homojunction counterparts.

High performance electronic and photonic devices that incorporate heterostructures, such as those mentioned above, have been realized due to recent advances in epitaxial growth techniques such as molecular beam epitaxy (MBE) and metal-organic chemical vapor deposition (MOCVD). These advanced epitaxial growth techniques are low-temperature in nature and permit atomic level control over the deposition process enabling heterostructures to be grown having extremely abrupt interfaces.

A particular advantage of modern epitaxial growth techniques is that they can be employed to integrate materials having different properties in a monolithic fashion within limits imposed by factors such as lattice-mismatch and thermal stability. An example of materials integration would be the GaAs/Si epitaxial system, where photonic devices fabricated in GaAs could be integrated monolithically with Si electronic devices. A second example of materials integration concerns the subject of this dissertation, namely the $In_xGa_{1-x}As$/GaAs epitaxial system.

The work to be described was motivated by the idea of monolithically integrating photonic devices fabricated in $In_xGa_{1-x}As$ with GaAs integrated circuits (ICs). Such a scheme is interesting in principle due to the following reasons: Firstly, GaAs IC technology is rapidly advancing to the point, for example, that high-speed GaAs logic elements have been incorporated in Cray computers. And secondly, the $In_xGa_{1-x}As$ ternary system has a direct-bandgap range from 1.42eV (x=0) to 0.36eV (x=1). This bandgap range would correspond to photonic devices operating in the, 0.87μm (x=0) to 3.4μm (x=1), wavelength range. Such a wavelength regime encompasses several important wavelengths. For instance, wavelengths of 1.3 and 1.55μm represent the dispersion and absorption minima, respectively, in the case of silica glass fibers and also fluoride-based fibers appear to have an attenuation minimum around 2μm.

Hindering the growth of device quality $In_xGa_{1-x}As$ alloys on GaAs, however, are the large lattice-mismatch strains associated with this material system which lead to dislocation formation and thus the degradation of photonic devices. Control over dislocation propagation,

consequently, is of paramount importance and, hence, fundamental studies concerning this subject are required such that the $In_xGa_{1-x}As$/ GaAs material integration can become a reality.

The presently described work had two principal objectives. Firstly, the mechanisms responsible for strain relief in the $In_xGa_{1-x}As$/GaAs heteroepitaxial system were to be identified as a function of $In_xGa_{1-x}As$ composition, covering as wide a composition range as possible. Secondly, a composition range was to be identified over which low-dislocation density $In_xGa_{1-x}As$ material could be grown either directly or indirectly on GaAs.

Prior to outlining the scope of the present work, a discussion section follows on the literature as it pertains to this dissertation.

1.2 Background

Lattice-mismatch strain presents the greatest obstacle towards the growth of high quality $In_xGa_{1-x}As$ on GaAs. The lattice parameter of $In_xGa_{1-x}As$ is larger than that of GaAs with the mismatch strain reaching 7% when x=1 [1]. Therefore, in the $In_xGa_{1-x}As$/GaAs system, the epilayer experiences in-plane biaxial compression since the epilayer lattice tries to conform to that of the substrate until an elastic limit is reached and strain relaxation occurs. The following section reviews the published literature on strain, strain relief and dislocation evolution in lattice-mismatched systems in general, with particular reference to the $In_xGa_{1-x}As$/GaAs material system. Also, various buffer structures used to block dislocations in such lattice-mismatched systems are reviewed.

1.2.1 Critical Thickness in Lattice-Mismatched Systems

In the case of heteroepitaxial systems in which the lattice-mismatch is small, the first atomic layers that are deposited during epitaxial growth will be strained to match the substrate lattice (pseudomorphic growth) and a coherent interface is formed. However, as the thickness of the epilayer increases, the homogeneous strain energy in the epilayer becomes large enough to allow the nucleation of misfit dislocations at the heterointerface. The thickness of the epilayer at which misfit dislocations are nucleated corresponds to the critical thickness for that epilayer/substrate material system. In this section several models used to predict critical thickness are discussed, and published experimental data on critical thicknesses in the $In_xGa_{1-x}As/GaAs$ material system are presented.

Van der Merwe [2] proposed a model to predict the critical thickness of a lattice-mismatched epilayer/ substrate system by equating the areal strain energy density in the epilayer to the interfacial energy per unit length between the epilayer and the substrate arising as a result of the generation of misfit dislocations. The interfacial energy was evaluated using the Peierls-Nabarro potential to represent the interatomic forces at the interface. Such a calculation of the interfacial energy, however, becomes significantly inaccurate when the misfit dislocation spacing is greater than twice the epilayer thickness leading to a conservative estimate of the critical thickness.

Using a different approach than that employed by Van der Merwe [2], Matthews [3-5] calculated the critical thickness by minimizing the elastic (coherent) and plastic (dislocation) energy terms. This is equivalent to a mechanical equilibrium of forces acting on a dislocation. Matthews [3-5] assumed that the lattice-mismatch is accommodated by a regular array of non-interacting edge dislocations and that a misfit dislocation is formed by the bowing of grown-in threading dislocations, such that a segment of the dislocation line lies parallel to the interface. The forces acting on a threading dislocation are the line tension and the force due to mismatch stress at the interface. In the initial coherent layer the line tension force is larger than the force due to the mismatch stress. As the epilayer thickness increases, the force due to the mismatch stress increases and at the critical thickness is equal to the line tension force. This mechanism, however, becomes inaccurate for small lattice-mismatch strains due to the low density of grown-in threading dislocations.

Recently, People and Bean [6,7] followed a procedure similar to that of Van der Merwe [2] to evaluate critical thicknesses of lattice-mismatched systems. These authors assume that the growing epilayer is initially free of threading dislocations and that the interfacial misfit dislocations are generated when the areal strain energy density in the epilayer exceeds the self energy of an isolated dislocation at the interface. The energy balance is considered over a region of the coherently strained lattice equal to the width of the dislocation strain field. There are three problems associated with People and Bean's [6,7] calculations. Firstly, the energy of an isolated screw dislocation in an infinite crystal lattice is used to represent the energy of a

dislocation in a finite epilayer. Secondly, the interface consisting of two vastly different materials (in terms of mechanical properties) is considered to have similar properties as that of a bulk epilayer material. Thirdly, an effective interfacial width of only four to five <110> atomic spacings is used to determine the energy of the dislocation which is inaccurate for small lattice-mismatched systems. The aforementioned factors lead to a gross overestimation of the critical thickness.

Several experimental studies concerning critical thickness measurements in the $In_xGa_{1-x}As/GaAs$ system performed using various analytical techniques have been published in the literature [8-13] and the reported data are illustrated in Figure 1-1 together with the theoretical predictions of Van der Merwe [2], Matthews [3-5] and People and Bean [6,7]. Orders and Usher [9] determined lattice parameters of $In_xGa_{1-x}As$ (x=0.07,0.14 and 0.25) layers of various thicknesses grown on GaAs substrates using x-ray rocking curve analysis and denoted the critical thickness (h_c) to be the layer thickness at which the lattice parameter changed abruptly to its relaxed value. Their [9] determination of critical thicknesses seemed to agree with the theoretical predictions of People and Bean [6,7] (Figure 1-1) for $In_xGa_{1-x}As$ compositions of x=0.14 and x=0.25.

Another critical thickness study was reported by Fritz et al. [10] who performed photoluminescence (PL) microscopy on $In_{0.2}Ga_{0.8}As$ layers of various thicknesses grown on GaAs. The PL micrographs showed the presence of dark-line defects for epilayer thicknesses greater than 20nm. As can be seen from Figure 1-1 this value of

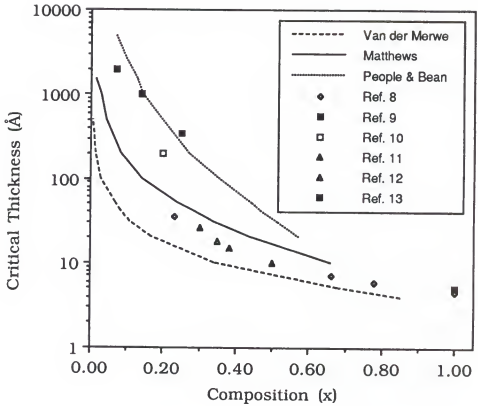

Figure 1-1. $In_xGa_{1-x}As/GaAs$ epilayer critical thickness data reported by various authors [8-13] as a function of $In_xGa_{1-x}As$ composition. Also shown are theoretical plots based on three models [2-7].

critical thickness lies between the curves predicted by Matthews [3-5] and People and Bean's [6,7].

Nakao and Yao [8] performed in-situ reflection high energy electron diffraction (RHEED) during molecular beam epitaxial (MBE) growth of $In_xGa_{1-x}As$ layers (x=0.23, 0.66, 0.78 and 1) on GaAs and measured the surface lattice parameter of the epilayers from the spacing between reciprocal rods as a function of epilayer thickness. At the critical thickness, the surface lattice parameter abruptly changes from the substrate (coherent) to the bulk epilayer (relaxed) value. Similar investigations were conducted by Price [11] for $In_xGa_{1-x}As$ layer compositions of x=0.3, 0.38 and 0.5 and by Berger et al. [12] for x=0.35. All the experimental values are shown in Figure 1-1 and the data points lie between Matthew's [3-5] and Van der Merwe's [2] theoretical models for the evaluation of critical thickness. In a recent study, Price [14] showed that the critical thickness of $In_xGa_{1-x}As$ is a strong function of the temperature employed in epitaxial growth. Price [14] observed that for an $In_{0.35}Ga_{0.65}As$ epilayer grown on GaAs by the MBE technique, the critical thickness increases with decreasing growth temperature. Price [14] also showed that the surface lattice parameter shows a gradual increase with increasing thickness until a critical growth temperature is reached when the lattice parameter increases abruptly at a critical thickness. Ideally, during the epitaxial growth process, the epilayer grows one atomic layer at a time (2D growth). In order to achieve this ideal growth condition, the surface mobility of the atoms should be large so that they can migrate to an atomic ledge on the surface and allow for uniform coverage throughout the monolayer. However, if the lattice-

mismatch is large (>2%) [11], the mismatch strain might significantly decrease the surface mobility. Also, if the growth temperature is low, the surface mobility of atoms is significantly reduced. Therefore in scenarios of large lattice mismatch strains and/or low growth temperatures, island (3D) growth occurs. Island growth allows for a larger areal strain energy than 2D growth and hence the observed larger critical thickness at lower growth temperatures. The growth temperature at which the surface lattice parameter shows an abrupt change is denoted as the 3D-2D growth transition temperature. Other published results [12,15-17] of similar RHEED studies on $In_xGa_{1-x}As$ epilayers as a function of the growth temperature report similar observations and use the 2D-3D growth transition temperature concept to explain the observations.

In summary, the experimental data reported in the literature suggest that the onset of strain relief (critical thickness) in the $In_xGa_{1-x}As/GaAs$ system does not conform precisely to any of the available theoretical models concerning the prediction of critical thickness. Also, the critical thickness of $In_xGa_{1-x}As/GaAs$ epilayers appears to be sensitive to the growth temperatures employed.

1.2.2 Strain Relief Mechanisms

Strain relief occurs in lattice-mismatched systems by the evolution of dislocations when the epilayer thickness reaches a critical value. In this section, the published literature on proposed models for strain relaxation and experimental results concerning the $In_xGa_{1-x}As/GaAs$ material system are discussed.

Matthews and Blakeslee [18] proposed a model to predict the extent of strain relaxation by considering an equilibrium of stresses acting on a threading dislocation. The stress exerted by the lattice mismatch strain on a dislocation (σ_e) in its glide plane and the effective stress due to the dislocation line tension (σ_l) are given by

$$\sigma_e = \frac{2\mu e\,(1+\nu)}{1-\nu}$$

and

$$\sigma_l = \frac{\mu}{2\pi}\,\frac{\left(1-\frac{\nu}{4}\right)}{1-\nu}\,\frac{1+\ln\left(\frac{h}{b}\right)}{h/b}$$

where μ is the shear modulus, ν is the Poissons ratio, b is the Burgers vector and h is the thickness of the epilayer. The two stresses are equated to give the residual strain in the epilayer

$$e_{eq} = \frac{b}{4\pi}\,\frac{\left(1-\frac{\nu}{4}\right)}{(1+\nu)}\,\frac{1+\ln\left(\frac{h}{b}\right)}{h}$$

where e_{eq} is the equilibrium residual strain in the epilayer.

A second model proposed by Tsao et al. [19] suggests that the driving stress for dislocation motion is the difference between the stress due to misfit strain (σ_e) and the effective stress due to the dislocation line tension (σ_l) and an observable strain release should occur only if this "excess" stress (σ_{ex}) exceeds a critical value which depends on the growth temperature.

$$\sigma_{ex} = \sigma_e - \sigma_l$$

Using the excess stress a shift from the equilibrium residual strain value was given by

$$e_m = e_{eq} + \frac{\sigma_{ex}(1 - \nu)}{2\mu(1 + \nu)}$$

Since the value of σ_{ex} is unknown, a number of plots of e_m versus h for various values of the excess stress are used to obtain a fit to experimental data unique to a lattice-mismatched system.

Another model for strain release was proposed by Dodson and Tsao [20,21] assuming that strain relaxation is limited by the kinetics of dislocation movement and multiplication. Without going into the mathematics, the final result is a differential equation given by

$$\frac{d\gamma(t)}{dt} = C\mu^2 [f - \gamma(t) - e_{eq}]^2 [\gamma(t) + \gamma_0]$$

where $\gamma(t)$ is the time-dependent strain release, e_{eq} is the equilibrium strain, γ_0 is a source term which accounts for the density of threading dislocations in the substrate, f is the misfit strain and C is a phenomenological parameter which contains the dislocation-glide velocity. Due to the term, C, the strain relaxation should depend on the growth velocity, i.e. the time the specimen is held at the growth temperature.

Using a different approach, Maree et al. [22] explained strain relaxation in the epilayer by means of surface nucleation and expansion of dissociated half loops while taking into account the misfit stress field acting on expanding loops. The half loop energy (E_h) increases with increasing loop radius (r), reaches a maximum value when $dE_h/dr=0$ at a critical radius r_c and then decreases with further

dislocation loop expansion. In the case of an in-plane compressive strain (as in the $In_xGa_{1-x}As/GaAs$ system), the residual strain in the epilayer (e) is given by

$$e^2 = \frac{b\left(1 - \frac{\nu}{2}\right)}{240h(1+\nu)}\left[\ln\left(\frac{4r_c}{b}\right) - \frac{1}{2}\right]$$

In order to determine the model that best predicts the extent of strain relaxation, Drigo et al. [23] performed a study of the residual strain in MBE grown $In_xGa_{1-x}As$ (x=0.035, 0.08, 0.10 and 0.15) epilayers of various thicknesses grown on GaAs. The parallel or in-plane lattice-mismatch residual strain was determined using Rutherford backscattering/channeling spectrometry. The results showed that the measured residual in-plane strain, represented by data points and a best fit to the data denoted by a dotted line in Figure 1-2a, is much larger than predicted by the Matthews and Blakeslee [18] equilibrium model represented by the solid line in Figure 1-2a. The experimentally determined values for residual strains did not agree with those predicted by Tsao et al. [19] (Figure 1-2b). The residual strain data, however, appears to fit the energy-balance model proposed by Maree et al. [22] based on the nucleation of half-loops (Figures 1-2b). An annealing study at the growth temperature was conducted in order to observe if further strain relief occurred with increasing the time at the growth temperature as proposed by Dodson and Tsao [20,21]. The results showed no further strain relief thus discounting Dodson and Tsao's model [20,21] for strain relief in the $In_xGa_{1-x}As/GaAs$ system. Strain relief data obtained from $In_xGa_{1-x}As$ layers by Kamigaki et al. [24] for x=0.082-0.2 and Orders and Usher [9]

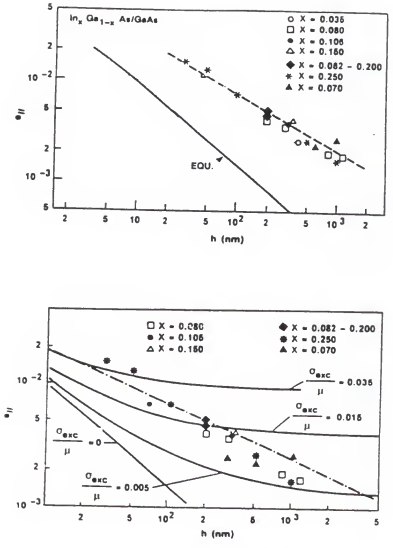

Figure 1-2. A plot of the experimental data from studies [9,22-24] on the in-plane residual strain (e) as a function of thickness (h) and its correlation to proposed models for strain relaxation.
a) The dashed line represents a best fit to the experimental data while the solid line represents the equilibrium model [18] showing that the model overestimates the extent of strain relaxation; b) The solid lines represent the predictions of Tsao et al.'s [19] model for various values of the excess stress and show no correlation to the experimental data. The dot-dashed line represents the results of the energy-balance model for the nucleation of half-loops [22] and provides a good correlation to the experimental data points. (From Drigo et al. [23])

for x=0.25 by x-ray diffraction and Maree et al. [22] for x=0.07 by ion blocking are also shown in Figures 1-2a and 1-2b. These data points also fit the energy balance model based on the nucleation of half loops.

In summary, as far as the literature is concerned the strain relaxation model based on half loop nucleation and expansion appears to best represent the extent of strain relaxation in the $In_xGa_{1-x}As/GaAs$ material system.

1.2.3 Dislocation Evolution in the $In_xGa_{1-x}As/GaAs$ Material System

In order to nucleate dislocations, either the stress in the epilayer/substrate system requires to reach a value that is favourable to nucleate dislocations for homogeneous nucleation or there has be a dislocation source such as a stress concentrator to allow for the heterogeneous nucleation of dislocations. There are various possible sources that could act as stress concentrators for dislocation formation in lattice-mismatched systems.

The first candidates for dislocation sources as suggested by Matthews et al. [3] are threading dislocations that replicate from the substrate and penetrate the strained epilayer (Figure 1-3a). Such dislocations will produce misfit dislocations when $\sigma_{ex}>0$, i.e. the mismatch stress is greater than the dislocation line tension. The relaxation rate is proportional to the velocity of the threading dislocation gliding due to the excess stress.

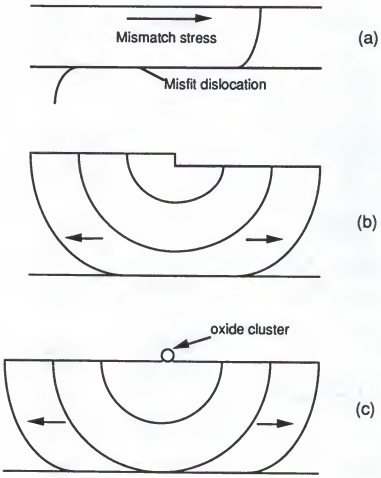

Figure 1-3. Schematic diagram of possible sources of misfit dislocations.
a) Generation of misfit dislocations from grown-in threading dislocations; b) Homogeneous nucleation of dislocation half loops at surface steps; c) Heterogeneous nucleation of dislocations at stress concentrators such as an oxide inclusion which could act as dislocation mills.

Another possibility is the homogeneous nucleation of dislocation half loops at the surface (Figure 1-3b). In order to activate such a source at the surface, the physical stress at the surface must be large enough to nucleate dislocation half loops. This process has been addressed by several authors [25-27] and the concensus is that a lattice-mismatch strain of several percent would be required to nucleate dislocations at such surface steps.

A third possibility would be the local formation of dislocation mills, similar, in principle, to a Frank-Read source [26] (Figure 1-3c). The mechanism of dislocation mills involves the expansion of a dislocation structure until an unbound dislocation loop pinches off, leaving behind the original dislocation structure which is then free to generate more dislocation loops.

Fitzgerald et al. [28,29] performed an extensive study of dislocation generation specifically on 1μm thick $In_xGa_{1-x}As$ (x=0.12) epilayers grown on GaAs using plan-view and cross-sectional TEM analyses. Plan-view TEM analysis of the $In_xGa_{1-x}As$/GaAs heterointerface showed a dislocation network made up of 60° a/2<110> mixed dislocations. Since $In_xGa_{1-x}As$ has a zincblende-type structure, perfect dislocations in the lattice have an a/2<110> type Burgers vector. Of the three main types, namely, edge, screw or 60° mixed dislocations, the edge type has the highest core energy and the screw type cannot relax a tetragonal lattice mismatch, leaving the 60° mixed type as the most probable dislocation to form in $In_xGa_{1-x}As$ layers [30].

Furthermore, cross-sectional TEM analysis of the heterostructure showed the presence of dislocation half-loops in the

GaAs substrate and an absence of dislocations in the $In_xGa_{1-x}As$ epilayer. The three types of dislocation sources mentioned earlier, namely, threading dislocations, homogeneous nucleation at the surface steps and heterogeneous nucleation or dislocation mills at the surface which when active would cause threading dislocation formation in the epilayer are obviously not active in the $In_xGa_{1-x}As$ (x=0.12)/GaAs system since dislocations are not observed in the $In_xGa_{1-x}As$ epilayer. Fitzgerald et al. [28,29] attributed the absence of dislocations in the epilayer to a larger misfit strain in the epilayer compared to the substrate. However, observations in other lattice-mismatched systems such as ZnSe/GaAs [31] and GaAs/Si [32], where the misfit strain in the epilayer is larger than that in the substrate, do not conform to Fitzgerald et al.'s [28] explanation since, in these material systems, dislocations are, in fact, observed in the epilayer.

Fitzgerald et al. [28] also proposed a model to predict the extent of dislocation propagation into the substrate by considering a balance of forces acting on a dislocation in the GaAs at a distance x along {111} planes from the heterointerface. This distance, x, is correlated to a depth of penetration of a 60° dislocation into the substrate by straight forward geometrical considerations. In this model, a Peierls force (F_p), an image force (F_i), a line tension force (F_l) and a force from the elastic strain in the substrate (F_e) act on a dislocation to prevent it from moving further into the substrate and repulsion forces (F_d) from 60° dislocations having the same Burgers vector act to move the dislocation into the substrate. At the equilibrium distance, x,

$$F_d = F_e + F_i + F_l + F_p.$$

Fitzgerald et al. [28] showed that the calculated value for penetration depth of a dislocation into the substrate agrees with the experimental values determined using XTEM.

Chang et al. [33,34] conducted PTEM and XTEM analyses on $In_xGa_{1-x}As$ (x=0.15, 0.3 and 0.5) layers grown on GaAs. PTEM analysis of the heterostructures showed that the dislocations were mostly 60° a/2<110> mixed type in character at the $In_{0.15}Ga_{0.85}As$/GaAs heterointerface. However, analysis of the $In_{0.3}Ga_{0.7}As$ and $In_{0.5}Ga_{0.5}As$ alloys revealed predominantly edge type dislocations. The increase in edge type dislocations with increasing lattice-mismatch was attributed to island growth since island coalescence normally leads to the formation of edge dislocations. XTEM analysis of these particular $In_xGa_{1-x}As$/GaAs structures showed the absence of dislocations in the $In_{0.15}Ga_{0.85}As$ epilayer and the presence of a large number of threading dislocations in the $In_{0.3}Ga_{0.7}As$ and $In_{0.5}Ga_{0.5}As$ epilayers. Chang et al. [33] suggested a 2D-3D growth mode transition due to large lattice-mismatch strains (>2%) to explain the appearance of threading dislocations in x>0.15 epilayers. Such an explanation, however, does not appear to be valid since studies on material systems which contain much smaller lattice-mismatches and therefore have a 2D growth mode, for example the ZnSe/GaAs material system [31], show threading dislocations in the epilayer unlike $In_xGa_{1-x}As$/GaAs layers with similar lattice-mismatch strains. Also, RHEED and TEM studies conducted by Tabuchi et al. [35] on the $In_xGa_{1-x}As$/GaAs system (x=0.2, 0.3, 0.4, 0.5, 0.7 and 1) show that despite an observed 2D growth mode for $In_xGa_{1-x}As$ epilayers with

$x<0.5$, threading dislocations form in $In_xGa_{1-x}As$ epilayers of $x>0.2$. Therefore, the 2D-3D growth mode transition mechanism as a means to explain the onset of threading dislocation formation in $In_xGa_{1-x}As$/GaAs layers appears to be invalid for epilayers with x values less than 0.5. Tabuchi et al. [35] stated that island growth occurs in $In_xGa_{1-x}As$/GaAs systems with $x>0.5$. Also, Guha et al. [36] conducted high resolution XTEM analysis on extremely thin layers of $In_{0.5}Ga_{0.5}As$ grown on GaAs and directly observed the formation of islands. Therefore, it appears that for $x\geq0.5$, island formation and coalescence could contribute to threading dislocation formation in $In_xGa_{1-x}As$ epilayers.

In summary, it seems clear that current postulates which are designed to explain the nature of dislocation sources and dislocation evolution in lattice-mismatched systems are not adequate to completely account for dislocation evolution in the $In_xGa_{1-x}As$/GaAs material system.

1.2.4 Common Buffer Structures Used to Block Dislocations

Various schemes have been studied by various authors [37-40] with a view towards reducing the threading dislocation density in lattice-mismatched $In_xGa_{1-x}As$ layers grown on either GaAs or InP. The techniques that have been employed to minimize the effects of lattice-mismatch can be summarized as follows:

a) Growth of a continuously graded $In_xGa_{1-x}As$ buffer layer [38] on InP such that the lattice parameter (corresponding to a layer composition of $In_{0.53}Ga_{0.47}As$) adjacent to the substrate was matched to that of

InP and the lattice parameter (and composition) at the top of the buffer was matched to that of an $In_{0.77}Ga_{0.23}As$ epilayer of interest. Reduction in dislocation density via use of the buffer, however, was very insignificant (less than an order of magnitude).

b) Step graded growth where thin $In_xGa_{1-x}As$ layers (~2000Å each) with increasing composition (x=0.25, x=0.5 and x=0.75) are grown on GaAs in a stacked manner, resulting in partial confinement of the misfit dislocations at intermediate interfaces [37,39]. Reductions in dislocation densities by up to 2 to 3 orders of magnitude were achieved by this method in the case of heteroepitaxy of InAs on GaAs.

c) Growth on patterned GaAs substrates where substrates are etched to form mesas and trenches and misfit dislocations form, upon growth of an $In_{0.05}Ga_{0.95}As$ layer, by the nucleation of half-loops which appear to glide along the interface leaving a strain relieving dislocation behind [41,42]. These dislocations glide from the mesas into the trenches but appear to be blocked from gliding into adjacent mesas leaving the mesas relatively dislocation-free. However, $In_xGa_{1-x}As$ layers with larger lattice-mismatches to GaAs require to be studied in order to justify the use of this scheme since, as has been detailed earlier, such small x ($x \leq 0.15$) $In_xGa_{1-x}As$ layers can be grown directly on GaAs without the introduction of threading dislocations in the epilayer.

d) Growth of strained layer superlattices (SLSs) are also used to act as barriers to dislocation motion. SLSs are the most widely employed structures designed to block dislocations and hence the remainder of this section is devoted to the principles of dislocation blocking by

SLSs, in general, and to a discussion on the experimental studies specific to the $In_xGa_{1-x}As/GaAs$ material system.

El-Masry et al. [43] have studied dislocation interactions within an $In_xGa_{1-x}As/GaAs$ SLS system and report that the 60° mixed dislocations are bent inside the SLS and their direction is changed towards one of the <110> directions along the SLS interfaces. These authors suggest that effective bending of dislocations requires that all threading dislocations experience a gliding force known as the Peach-Koehler force whose magnitude depends on the strain and layer thickness.

Matthews and Blakeslee [18], in general, have suggested that a minimum layer thickness in the SLS is required in order to bend threading dislocations, their theory being based on the existence of a finite stress in individual layers of the SLS acting to bend over and confine threading dislocations. The critical minimum thickness is therefore dependent on the strain between the individual layers in the SLS.

In general terms, the lattice-mismatch in a SLS results in a biaxial state of stress for the individual layers. Assuming isotropic behaviour, the shear stresses and shear strains are equal to zero along the {100} planes. However, finite resolved shear stresses exist in {111} planes along <110> directions which are the slip planes and slip directions, respectively, for 60° mixed type dislocations which are the most common of the dislocation types observed in lattice-mismatched systems. For relatively small shear stresses dislocations would continue to thread into the epilayer, hence rendering the SLS ineffective; however, for relatively large stresses which are sufficient

to bend dislocations, a significant reduction in dislocation density can be achieved when the majority of the dislocations are of the mixed type.

Interactions between adjacent dislocations may occur if the density of dislocations penetrating the SLS is very large ($10^8/cm^2$). These interactions depend on the stress field around the dislocations and the distance between adjacent dislocations. If an attractive stress field exists between two dislocations they can interact to form one dislocation or a half loop, thus reducing the dislocation density.

Favourable conditions for dislocation reduction would be realized when 1) the dislocation is bent at the SLS interface and propagates to the sample edge, 2) two dislocations interact to cancel each other and form a half loop and 3) two dislocations react to form a third dislocation at a node.

Several studies [30,44,45] of dislocation evolution in $In_xGa_{1-x}As/GaAs$ (x=0.08-0.35) SLSs grown on GaAs using XTEM analysis have been conducted and the results suggest that most of the dislocations are confined to the SLS/GaAs heterointerface and the GaAs substrate, with only a few dislocations penetrating the superlattice. Also, it appears that the interactions of 60° misfit dislocations lead to the formation of edge dislocations at the nodes. The use of such low In content ($x<0.4$) $In_xGa_{1-x}As$ layers in $In_xGa_{1-x}As/GaAs$ superlattices could allow for the growth of high quality lattice-matched layers of $In_xGa_{1-x}As$ with x values <0.2. However, as discussed in earlier sections, such low dislocation density $In_xGa_{1-x}As$ layers ($x<0.2$) can be grown directly on GaAs without the use of SLSs. In other words, SLS buffer layers would appear to be

unnecessary for dislocation density reduction in $In_xGa_{1-x}As$ layers for x values <0.2.

1.2.5 Summary

A detailed review of published literature on the $In_xGa_{1-x}As/GaAs$ system suggests that currently available theoretical models for predicting critical thicknesses in lattice-mismatched systems are not suitable to explain the onset of strain relaxation in the $In_xGa_{1-x}As/GaAs$ material system. However, the extent of strain relaxation in this system appears to obey the theoretical model of Maree et al. [22] based on the surface nucleation and expansion of half loops.

Also, published studies on dislocation evolution in the $In_xGa_{1-x}As/GaAs$ system suggest an absence of dislocations in the epilayers for x<0.2. However, current postulates concerning the nature of dislocation sources and dislocation evolution are not adequate to explain dislocation nucleation and evolution in this material system.

1.3 Scope of the Present Work

The present work is detailed in five following chapters. In chapter 2, the growth techniques employed in the fabrication of single and multilayer $In_xGa_{1-x}As$ structures on GaAs are discussed along with the analytical techniques used to characterize the various heterostructures.

Chapter 3 details a dislocation evolution study performed on single $In_xGa_{1-x}As$ layers of various compositions grown on GaAs. Dislocation formation is explained based on the high temperature mechanical properties of the epilayers and the substrate. A unique concept of "critical composition" is proposed based on a balance of forces model which includes a surface image force to explain dislocation evolution in the $In_xGa_{1-x}As/GaAs$ material system.

In chapter 4, the step by step development of a multistage strain relief buffer employing conventional dislocation blockers, i.e. strained layer superlattices, for the growth of $In_xGa_{1-x}As$ layers with x values greater than 0.2 is discussed. The lattice-matching between individual layers in the multistage system is also detailed and the advantages and disadvantages of using such a buffer system are discussed.

Chapter 5 details a study of strain relaxation in single $In_xGa_{1-x}As/GaAs$ layers, the results of this study being applied towards the development of a multilayer system which permits the growth of extremely low-dislocation density $In_xGa_{1-x}As$ for x values up to 0.5. The multilayer design is based on an experimentally determined "critical compositional difference" associated with adjacent layers of a stacked $In_xGa_{1-x}As$ multi-layer system. The stacked systems consist of relatively thick $In_xGa_{1-x}As$ layers and do not employ conventional dislocation blockers, i.e., strained-layer superlattices.

In chapter 6, a summary of the important conclusions drawn from this study is provided along with recommendations for future research in this area.

CHAPTER 2
GROWTH AND CHARACTERIZATION TECHNIQUES

The various single and multiple layer $In_xGa_{1-x}As/GaAs$ heterostructures studied in this work were grown using the molecular beam epitaxy (MBE) technique by Dr. Y.W. Lin and Bruce Liu of our research group, while the heterostructures were designed by the author and characterized using various analytical techniques including cross-sectional and plan-view transmission electron microscopy (XTEM and PTEM), high-resolution x-ray diffraction (HRXRD), electron microprobe analysis and etch-pit analysis. The MBE growth conditions employed as well as the important considerations and procedures pertaining to the various characterization techniques mentioned above are outlined in the following chapter.

2.1 Molecular Beam Epitaxy

Molecular beam epitaxy is in essence a vacuum evaporation technique but with two important differences--the vacuum is ultrahigh vacuum (UHV) and the product of evaporation is a single crystal. In this technique, constituent elements and dopants are directed in the form of thermal molecular or atomic beams towards a heated single crystal substrate where epitaxial growth occurs. By monitoring the beam fluxes of the constituent elements, a precise compositional

control of the epitaxially growing layer is maintained. High purity source elements (in our case, In, Ga and As) are evaporated from high temperature effusion sources, the effusion sources being arranged about the heated crystalline substrate in such a way as to ensure uniformity both of composition and thickness. Rotation of the substrate during growth further facilitates the attainment of uniformity. The film composition is varied by altering the source temperatures, i.e. the temperature of the furnaces, thus varying the molecular beam fluxes. Additional control over the growth process is achieved by virtue of mechanical shutters associated with each individual source, the action of which either permits or prevents the beam from reaching the substrate.

With regard to the present work, the following characteristics of MBE make it an ideal technique for the growth of multiple layer $In_xGa_{1-x}As/GaAs$ structures.

1. In general the growth rate is low, less than 1μm/hr, i.e., around 1 monolayer/sec, which allows compositional or dopant changes to be made within atomic dimensions.

2. The low growth temperatures involved minimize interdiffusion effects.

3. Sequential deposition of different materials is possible thus preserving the chemical and structural integrity of the various interfaces.

4. The UHV environment allows reflection high energy electron diffraction (RHEED) analysis to be employed so that the structural properties of the epitaxial layers can be monitored in real-time.

In this study a Varian GEN II MBE system was employed for the growth of $In_xGa_{1-x}As$ layers on GaAs substrates, a schematic of the growth chamber being shown in Figure 2-1. The GaAs substrates were typically oriented 2° off the (001) plane towards the (110) plane and prior to growth the substrates were exposed to a UV/ozone environment for ~2 minutes. This procedure resulted in the formation of a uniform thin oxide film on the substrate surface thus protecting it from contaminants.

After being exposed to UV/ozone, the substrates were attached to molybdenum blocks using indium, and the molybdenum blocks were then loaded into the buffer chamber of the MBE system via an entry/exit chamber which were pumped down to pressures of $<5x10^{-8}$ torr and $<1x10^{-7}$ torr, respectively. The molybdenum block containing the substrate was then transferred into the growth chamber where the oxide was desorbed by heating the substrate at 650°C for 5 minutes under an arsenic overpressure.

The various sources used in the growth of $In_xGa_{1-x}As$ layers included one elemental In source, two elemental Ga sources, labeled Ga1 and Ga2, and one tetramer arsenic (As_4) source. A 0.2μm thick GaAs buffer layer was grown homoepitaxially on the substrate prior to the growth of the various heterostructures at a growth temperature of 600°C.

All of the $In_xGa_{1-x}As$ layers were grown employing a beam equivalent pressure (BEP) ratio, i.e. the ratio of the combined fluxes of the group III elements namely, Ga and In, to the flux of the group V element, of 16-20. The fluxes of the group III elemental sources and their corresponding source temperatures selected to provide various

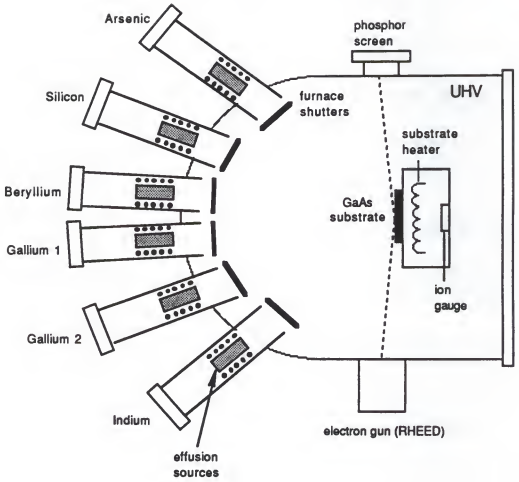

Figure 2-1. Schematic of MBE growth chamber configured for the growth of $In_xGa_{1-x}As/GaAs$ multiple layer systems. The Si and Be sources are n- and p-type sources, respectively.

$In_xGa_{1-x}As$ layer compositions are provided in Table 2-1. The substrate temperatures, i.e. growth temperatures, were optimized [46] with regard to growing stoichiometric $In_xGa_{1-x}As$ material and the various temperatures employed are given in Table 2-1. For the growth of $x \leq 0.22$ $In_xGa_{1-x}As$ layers the BEP of Ga was maintained at 5.33×10^{-7} while the BEP of In was altered to provide the requisite $In_xGa_{1-x}As$ layer composition. For $In_xGa_{1-x}As$ layer compositions in the range $0.22 \leq x \leq 0.4$, the beam equivalent pressure (BEP) of In was maintained at 2.26×10^{-7} torr while the Ga pressure was altered to provide the required epilayer composition. Above an x value of 0.4, the BEP of In was maintained at a slightly higher value of 3.33×10^{-7} torr in order to provide the larger amount of In needed for these compositions while the BEP of Ga was adjusted to provide the required composition.

The growth of multilayer structures consisting of layers of $In_xGa_{1-x}As$ with different compositions involves growth interrupts between layers consisting of two different compositions. During a growth interrupt, the substrate temperature is adjusted to correspond to that which is optimum for the growth of the subsequent layer. Also, the In source is shuttered and its temperature altered to provide the requisite beam flux for the growth of the next layer. If both Ga sources are in use, then they are both shuttered during the interrupt and their temperatures are adjusted to provide the required beam flux for the growth of the succeeding layer. However, if only one of the Ga sources is active during the growth of a layer then the idle or shuttered Ga source temperature is altered to provide the optimum layer composition for the subsequent layer so that at the growth interrupt,

Table 2-1. Optimized growth conditions employed in the growth of $In_xGa_{1-x}As$ layers on GaAs.

Composition (x)	Substrate temperature (°C)	Group III BEP ($x10^{-7}$torr)		BEP (V/III) Ratio
		In	Ga	
0.14	520	1.30	5.33	16-20
0.22	460	2.26	5.33	16-20
0.30	420	2.26	3.52	16-20
0.35	400	2.26	2.80	16-20
0.40	380	2.26	2.26	16-20
0.45	360	3.33	2.71	16-20
0.48	360	3.33	2.40	16-20
0.50	350	3.33	2.22	16-20
0.53	340	3.33	1.97	16-20

the idle Ga source is activated and the active Ga source is shuttered. This cycle is repeated at each growth interrupt encountered during the growth of a multilayer structure. Growth of the various layers is monitored using RHEED to ensure the structural integrity of the material. While a streaky diffraction pattern designates a material of good crystalline quality growing in a 2D or planar growth mode, a spotty pattern represents a rough surface caused by 3D or island growth.

After growth, the epilayer/substrate structures were removed from the MBE system, detached from the molybdenum blocks and extensively analyzed using the various techniques to be discussed below.

2.2 Characterization Techniques

The analytical techniques employed in this study included transmission electron microscopy, etch-pit analysis, electron microprobe analysis and high-resolution x-ray diffraction. In this section, details regarding the experimental procedures related to the various characterization tools are presented.

2.2.1 Transmission Electron Microscopy

The various $In_xGa_{1-x}As/GaAs$ heterostructures grown by MBE, as outlined in section 2.1, were analysed by cross-sectional and plan-view transmission electron microscopy (XTEM and PTEM) using a JEOL 200CX transmission electron microscope. XTEM was used to study

dislocation evolution in the heterostructures and PTEM analysis was used to determine dislocation densities in the top layers of stacked systems. XTEM and PTEM analyses were conducted using the various reflections available on (011) and (001) zones, respectively. In the following subsections, sample preparation techniques for XTEM and PTEM analyses are detailed.

2.2.1.1 Cross-sectional TEM specimen preparation technique

The MBE grown samples were cut into 10 mil thick strips using a dicing saw and the top surfaces, i.e. the MBE grown epilayer surfaces, of two of the strips were coated with M600 Bond epoxy resin and brought together in such a way that these coated surfaces were in close contact with each other. The coated strips were then heated for 45 minutes at 120°C in a conventional oven to cure and thus harden the epoxy resin. Such bonded strips were polished down to a thickness of about 50μm using a Struers polishing jig. A copper ring was then mounted onto the thinned specimen to provide mechanical stability. The specimen was thinned further in a Gatan two-stage ion mill using the sputtering action of two Ar^+ ion guns at a gun voltage of 5kV and a gun current of 0.5mA until a small hole was obtained. The regions in the vicinity of the hole were very thin and thus electron transparent and could be analysed in the TEM.

2.2.1.2 Plan-view TEM specimen preparation technique

After MBE growth, when a sample is detached from the molybdenum block, residual indium, which was used to bond the substrate to the block during growth, remains on the substrate side of the specimen. Therefore, the first step towards the preparation of a PTEM specimen involves polishing the substrate side of the sample until the indium is removed. The sample is then cleaved into square pieces in such a way that the diagonal length of each square is about 3mm. A coat of wax is then applied to the top surface of the sample to protect it during the etch. The sample is mounted on a holder and etched from the back surface in a jet etcher using a 1% bromine-methanol solution until an electron transparent region is obtained. The wax coat on the top surface is then removed using heptane or trichloroethylene and the specimen is ready for analysis.

2.2.2 Etch Pit Technique

Etch pit analysis was conducted on 1μm thick $In_xGa_{1-x}As$ top layers to determine the threading dislocation density. The etchant solution consisted of 1ml HF, 2ml H_2O, 8mg $AgNO_3$ and 1g CrO_3. Such a solution was used since it is sensitive to dislocation strain fields and thus preferentially etches those areas leaving etch pits behind. A count of the number of etch pits per unit area provides the dislocation density. By measuring the thickness of the epilayer remaining after 2, 4, 8, 15 and 30 second-etches, the etch-rate of the etching solution was determined to be about 500Å/second. The samples were etched

for 5 seconds and the dislocation density was determined by counting the number of etch pits in a 1cmx0.1cm area using a scanning electron microscope.

2.2.3 Electron Microprobe Analysis

Electron microprobe analysis was used to determine the composition, x, of single $In_xGa_{1-x}As$ layers grown on GaAs substrates. The specimens used for microprobe analysis consisted of $In_xGa_{1-x}As$ layers having thicknesses $\geq 1\mu m$. The electron microprobe technique involves the use of an electron beam to probe the surface of the sample. The electrons that impinge on the specimen generate x-rays which are characteristic to the elements comprising the material. An electron gun voltage of only 6kV was used in order to limit the beam penetration to the epilayer. Integrated x-ray peak intensities of the various elements were evaluated and normalized to those from reference specimens, i.e. InAs and GaAs, to provide the composition of the $In_xGa_{1-x}As$ layer. An average of ten measurements across the surface of the specimen were made to evaluate the x value of the $In_xGa_{1-x}As$ epilayer. The error involved using this technique was estimated to be $\Delta x \leq 0.005$.

2.2.4 High Resolution X-Ray Diffraction

High resolution x-ray diffraction (HRXRD) analysis was performed on $In_xGa_{1-x}As/GaAs$ heterostructures using a Phillips 5-crystal x-ray diffractometer. Since HRXRD is a relatively new research

tool, a brief discussion of the diffractometer set-up is detailed below. In the second subsection below, the optimization procedures required to obtain representative HRXRD rocking curves are outlined while the various steps involved in the measurement of strains in lattice-mismatched systems, such as the $In_xGa_{1-x}As/GaAs$ material system, are discussed in the third subsection.

2.2.4.1 Phillips high resolution x-ray diffractometer

The Phillips HRXRD system includes an x-ray source, a monochromator/ collimator, a goniometer and a detector. The x-ray source is a Cu target anode which is bombarded by accelerated electrons created at a cathode using a generator operating at 40kV. Upon such bombardment, the Cu target emits $CuK\alpha$ x-ray radiation at a characteristic wavelength of 1.54Å. The x-ray beam thus created has a broad angular and wavelength range and needs to be monochromatized and collimated prior to its impingement upon the specimen. The monochromator/collimator used in the Phillips system consists of four highly perfect germanium crystals (Figure 2-2). The crystals are cut in such a way that either their (440) or (220) planes could be used for diffraction. The crystals are aligned so as to reduce spectral dispersion and peak broadening of the incident x-ray beam. The first crystal (Figure 2-2) is set to the correct Bragg angle of the required diffracting plane (440 or 220) with respect to the incident $CuK\alpha$ x-ray beam. The schematic in Figure 2-2 shows three beam paths corresponding to different wavelength components of the dispersed

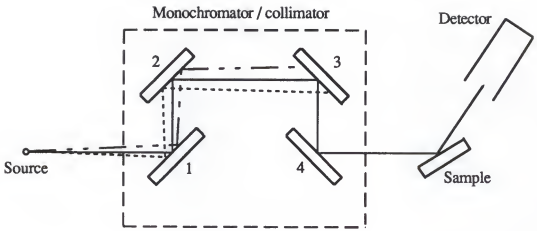

Figure 2-2. A schematic showing the alignment of the four Ge crystals in the monochromator/collimator section of the Phillips HRXRD system.

x-ray beam. All three components are diffracted simultaneously by the first crystal, but from different points on the crystal surface.

The second crystal is fixed in position such that it satisfies the Bragg condition for the median (solid line) wavelength component, but as shown in Figure 2-2 it also satisfies the Bragg conditions for other wavelength components. Therefore, there is no reduction in the spectral dispersion of the x-ray beam. However, the reflectivity (intensity of the diffraction beam about the Bragg peak) curve of the first and second crystals have an intrinsic angular width. The superposition of the reflectivity curves of the two crystals results in a reduction in the angular spread, thus collimating the x-ray beam. The third crystal is set in a non-parallel way, and only a small range of wavelengths can satisfy the Bragg condition for any fixed angle. The range of wavelengths passed through is related to the intrinsic rocking curve widths of the reflections used at the third crystal. Due to this drastic reduction in wavelength range, the x-ray beam that evolves is monochromatic in nature. The fourth and third crystals are aligned in the same manner as crystals one and two and hence a combination of crystals 3 and 4 serves to further collimate the x-ray beam. The alignment of the fourth crystal also serves in reflecting the x-ray beam back onto its original direction. An additional advantage of such a four crystal monochromator/collimator set-up is the ability to obtain rocking curves from any reflection of any single crystal specimen.

For Ge (440) planes, the intrinsic width of the diffracted beam is about 5 arc seconds allowing some 5% of the characteristic Kα line to pass. Therefore, the use of (440) reflections in the four Ge crystals provides an extremely monochromatic beam, however with very low

intensity (about 50,000 counts/second) requiring long x-ray scan times. For the Ge (220), the intrinsic width is larger than the (440) planes and is about 12 arc seconds, thus reducing the resolution of the diffractometer. However, the intensity of the exit x-ray beam from (220) planes is about 500,000 counts per second, hence requiring shorter scan times are required for the aquisition of x-ray data.

The x-ray beam, after passing through the monochromator/ collimator section impinges on a specimen mounted onto the sample stage in the goniometer. A schematic of the goniometer is shown in Figure 2-3. The goniometer has x,y and z cartesian coordinate controls for the adjustment of the sample stage position. The specimen is placed on the sample stage and the z axis of the stage is adjusted manually in such a way that the incident x-ray beam and the theta axis of the sample lie on a plane perpendicular to the plane containing the sample surface normal and the incident beam. The x and y axes of the sample stage are then adjusted via computer control so that the x-ray beam is incident on the specimen-area of interest.

The goniometer sample stage has three independent degrees of freedom for motion in spherical coordinate space. The sample can a) be rotated about its surface normal (z axis) over a $-170° < R < +170°$ range, b) be tilted about the x axis over a $-5° < Phi < +5°$ range and c) be rocked about the y axis over a $0° < 2\theta < 180°$ range. Furthermore, the detector can move independent of the goniometer over a 340° angular range. The angle between the detector and the sample surface is defined as $2\theta-\omega$ where ω is the angle between the fixed x-ray source and the sample surface. One's ability to rotate and tilt the specimen is utilized in terms of the optimization procedures to be discussed in the

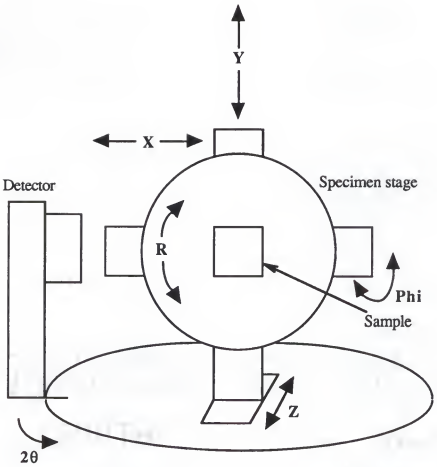

Figure 2.3: A schematic illustrating the various degrees of motion available on the goniometer sample stage used for x-ray rocking curve analysis of $In_xGa_{1-x}As/GaAs$ structures.

following subsection while one's ability to rock the specimen and move the detector independent of the specimen is utilized in the alignment of the diffractometer for the procurement of x-ray rocking curve scans.

As illustrated in Figure 2-4, two types of HRXRD rocking curve scans based on the variation of ω and/or 2θ were used in this work as follows:

a) The omega scan: where the detector is maintained stationary while the specimen rocks over a specified angular range as shown in Figure 2-4a. In this scenario, 2θ, which is the angle between the incident beam and the projected diffracted beam that reaches the detector remains a constant while the angle between the specimen surface and the x-ray source, ω, varies over a specified range. The ω scan is useful for the determination of the misorientation of a specimen whose Bragg condition is known. The 2θ value is fixed to satisfy Bragg's condition and thus at a certain value of ω (which need not necessarily equal θ) an x-ray peak is detected. This peak position can be used to determine the specimen geometry which will be discussed in detail in the following section.

b) The omega/2theta scan: where the range of ω is specified. However, the specimen is rocked over the specified angular range along with the detector which sweeps over the same range. The result is that the angular variation of 2θ is twice that of ω (Figure 2-4b). Such a scan where ω and 2θ can be individually specified is quite different from a $\theta/2\theta$ scan performed using a conventional diffractometer in which case only the θ value is specified and which cannot be used in cases where $\omega \neq \theta$. The $\omega/2\theta$ scan is used when the

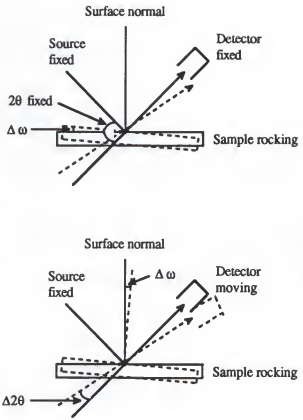

Figure 2-4. Schematics of the two types of HRXRD scans employed in the present study.
a) ω scan and c) ω/2θ scan.

specimen is composed of more than one material and the Bragg conditions of only one of the materials is known. The use of such a scan will be discussed in greater detail in a later section.

2.2.4.2 Optimization procedures

The GaAs substrates used for growth were typically miscut at 2° off the (001) plane towards the (110) plane. Therefore during an ω scan, the position of the GaAs x-ray peak often does not correspond to its real value, this value being $\omega=\theta$ for the symmetric (004) peak. A typical substrate miscut geometry is shown in Figure 2-5. As seen in the figure, as the specimen is rotated about its [001] normal direction, the position of the peak varies in the range $\omega-\Delta\alpha<\omega<\omega+\Delta\alpha$. This variation is sinusoidal, as shown in Figure 2-6, with a periodicity of 180°, the difference between maximum and minimum ω values corresponding to twice the misorientation.

A layer grown on a miscut substrate is also misoriented as seen in Figure 2-5, i.e. the surface normal does not correspond to the [001] direction. The variation of peak position, ω, for the epilayer is sinusoidal just as it is for the substrate. The misorientation of the epilayer, however, is not identical to that of the substrate as suggested by the differing values of maxima and minima for epilayer and substrate indicated in Figure 2-6. Such mistilts between epilayer and substrate have been reported for other epitaxial systems such as InP/GaAs [47,48], $Al_xGa_{1-x}As$/ GaAs [49] and ZnSe/GaAs[50-52]. The mistilts have been explained by a simple geometrical model assuming two-dimensional growth of the epilayer which starts at the substrate

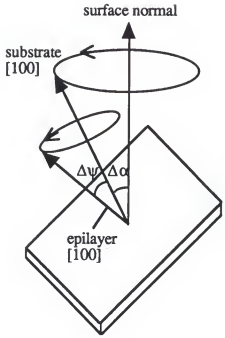

Figure 2-5. A schematic showing the substrate miscut, $\Delta\alpha$, and the epilayer mistilt, $\Delta\psi$, with respect to the surface normal.

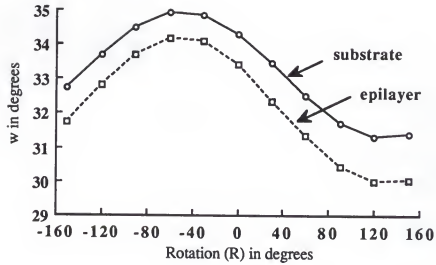

Figure 2-6. Plots of ω for substrate and epilayer as a function of specimen rotation angle, R, in an $In_{0.1}Ga_{0.9}As/GaAs$ structure showing a sinusoidal variation due to the substrate miscut (≈2°) and an epilayer mistilt (≈0.5°).

steps and grows in such a way that the epilayer surface normal (the growth direction) is tilted off the substrate normal and towards the (001) direction. This explanation appears valid for the $In_xGa_{1-x}As$/GaAs system since, as shown in Figure 2-6, the misorientation of the epilayer with respect to the [001] direction (deviation from optimal ω value) is less than that between the substrate and the [001] direction.

In order to obtain the true ω values for epilayer and substrate, the rotation angle has to be optimized. Since the Bragg angle of the epilayer is not known, ω scans are initially conducted at a fixed substrate Bragg angle (2θ fixed) and a optimal rotation angle for the substrate peak is obtained. An $\omega/2\theta$ scan is then performed about the substrate peak to determine the Bragg angle of the epilayer. This Bragg condition is used for further scans to optimize the epilayer peak value. In order to obtain accurate values for ω, the rotation needs to be optimized to an accuracy of 1°.

A second method for the determination of the real ω values involves the use of the known sinusoidal nature of the versus R curves. The sinusoidal variation implies that the real value for ω is the average of any two ω values separated by a rotation angle of 180°. Therefore, rocking curves performed at two rotation angles separated by 180°, say -90° and +90°, would be required to determine the real ω values for epilayer and substrate.

The intensities and widths of the various x-ray peaks are critically dependent on the angular orientation of the specimen with respect to the x-y plane, i.e. the tilt of the specimen shown in Figure 2-3. Since the positions of the peaks are not affected during optimization of the tilt angle, $\omega/2\theta$ scans can be used for this purpose.

The advantage of using such scans is that the Bragg conditions for both the epilayer and substrate peaks are satisfied in one scan. Therefore, a number of x-ray rocking curve experiments are performed at various tilt angles and the angle that provides the maximum peak intensity and minimum peak width is chosen as the optimum value.

The terminology for the peak positions used in the subsequent section represents the real peak positions after accounting for the miscut of the substrate and the mistilt of the epilayer.

2.2.4.3 Strain analysis using HRXRD

The peak position, ω, of the substrate peak at a symmetric plane, such as the (004) plane, (symmetric because the angle of incidence equals the angle of reflection as the sample surface is oriented to the (001) plane) can be used to determine the spacing, d, between the (004) planes from Bragg's law which is given by

$$n\lambda = 2d\sin\theta$$

where λ is the wavelength of the incident radiation and θ is the Bragg angle given by ω=θ for a symmetric reflection. The angular separation between substrate and epilayer peaks for the symmetric (004) reflection can be used to determine the perpendicular lattice-mismatch between epilayer and substrate given by

$$\left(\frac{a_{epi} - a_{sub}}{a_{sub}}\right)_{\perp} = -(\theta_{epi} - \theta_{sub})\cot\theta_{sub}$$

where a is the lattice parameter and the subscripts "epi" and "sub" stand for the epilayer and substrate, respectively.

In general one must distinguish between the mismatch perpendicular and parallel to the epilayer/substrate interface. These mismatch components can be determined by using HRXRD rocking curves from asymmetric lattice planes making an angle ϕ with the crystal surface. As shown in Figure 2-7, the Bragg condition for such a plane is satisfied at two different ω angles given by

$$\omega_1 = \theta + \phi$$

and

$$\omega_2 = \theta - \phi$$

From x-ray rocking curve scans, the values of ω_1 and ω_2 can be determined for both epilayer and substrate. By solving the aforementioned simultaneous equations, the values for θ and ϕ for both epilayer and substrate can be determined. A difference in lattice plane spacing between epilayer and substrate produces a difference, $\Delta\theta$, in the Bragg angle for a given {hkl} reflection, whereas a difference in lattice plane orientation corresponds to $\Delta\phi$. Assuming tetragonal distortion of the epilayer lattice, the perpendicular and parallel lattice-mismatches using an asymmetric {hkl} reflection can be evaluated as follows [53,54]:

Perpendicular lattice-mismatch:

$$\left(\frac{a_{epi} - a_{sub}}{a_{sub}}\right)_{\perp} = \Delta\phi \tan\phi_{sub} - \Delta\theta \cot\theta_{sub}$$

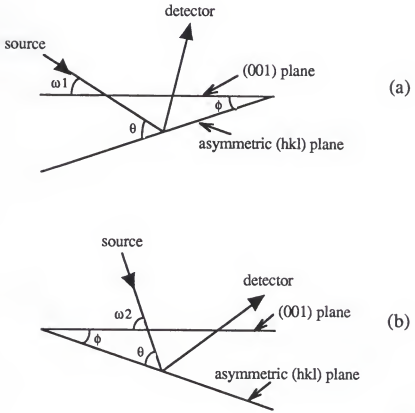

Figure 2-7. Schematics showing two conditions at which Bragg's law is satisfied for asymmetric planes that are at an angle, ϕ, to the symmetric (001) plane.
a) $\omega 1 = \theta - \phi$ and b) $\omega 2 = \theta + \phi$

Parallel lattice-mismatch:

$$\left(\frac{a_{epi} - a_{sub}}{a_{sub}}\right)_{\parallel} = -\Delta\phi\cot\phi_{sub} - \Delta\theta\cot\theta_{sub}$$

where $\Delta\theta$ and $\Delta\phi$ are given by

$$\Delta\theta = \theta_{epi} - \theta_{sub}$$

$$\Delta\phi = \phi_{epi} - \phi_{sub}$$

The difference between the perpendicular and parallel lattice-mismatches is related to the deformed epilayer unit cell. Another method to determine $\Delta\theta$ and $\Delta\phi$ is by solving simultaneously the peak separation equations from rocking curves obtained at ω_1 and ω_2 incidence, respectively, given by

$$\Delta\omega_1 = \Delta\theta + \Delta\phi$$

$$\Delta\omega_2 = \Delta\theta - \Delta\phi$$

where $\Delta\omega_1$ and $\Delta\omega_2$ are the peak separations at the two angles of incidence of the x-ray beam.

CHAPTER 3
STRAIN RELIEF IN $In_xGa_{1-x}As/GaAs$ SINGLE HETEROSTRUCTURES

3.1 Introduction

As discussed in the literature review section, theoretical and experimental studies conducted on the $In_xGa_{1-x}As$/ GaAs heteroepitaxial system have suggested that strain associated with the lattice-mismatch is relieved when the $In_xGa_{1-x}As$ epilayer thickness exceeds a critical value via dislocation formation and that the critical thickness is a function of the InAs mole fraction (x). However, as discussed in Section 1.2.3, currently published theories for dislocation evolution in lattice-mismatched systems are not adequate to explain the specifics of dislocation evolution in the $In_xGa_{1-x}As/GaAs$ material system. In this chapter, the results of an extensive strain relief study are detailed and a theory is presented to explain dislocation evolution in the $In_xGa_{1-x}As/GaAs$ heteroepitaxial system.

A set of $In_xGa_{1-x}As$ epilayers was grown on GaAs with a 0.5μm thick GaAs buffer being grown prior to $In_xGa_{1-x}As$ growth in each case. The $In_xGa_{1-x}As$ epilayers had InAs mole fractions of x=0.07, 0.14, 0.16, 0.18, 0.21, 0.28, 0.4 and 0.5 and were grown to a fixed thickness of 1μm which is well above the critical thickness for all of the compositions studied. Cross-sectional transmission electron microscopy (XTEM) analysis was performed on the $In_xGa_{1-x}As/GaAs$ single-layer structures in order to observe dislocation evolution as a

function of $In_xGa_{1-x}As$ composition. The XTEM studies were conducted using the various reflections available on the B[011] zone axis.

The following chapter is divided into three sections. The first section (3.2) deals with the experimental results from XTEM analysis of the various heterostructures while the second section (3.3) discusses the results and compares them to published reports. Finally, a novel theory is proposed in a third section (3.4) based on a balance of forces model which includes a surface image force term to explain dislocation evolution in the $In_xGa_{1-x}As/GaAs$ system.

3.2 XTEM analysis of $In_xGa_{1-x}As/GaAs$ Single Layer Structures

In order to facilitate an explanation of the observations regarding dislocation evolution, the $In_xGa_{1-x}As/GaAs$ structures are divided into three categories as follows:

$x < 0.18$	Small x structures
$0.18 < x < 0.28$	Medium x structures
$x > 0.28$	Large x structures

Cross-sectional TEM analysis of the small x structures indicated the absence essentially of threading dislocations in the $In_xGa_{1-x}As$ epilayer material as shown in Figure 3-1a. Threading dislocations are defined in this work as dislocations that traverse between the $In_xGa_{1-x}As/GaAs$ interface and the free surface. XTEM analysis of small x $In_xGa_{1-x}As/GaAs$ heterostructures revealed a dark band at the heterointerface along with dislocations in the GaAs substrate as shown in Figure 3-1b. A tilting experiment on such a structure showed the

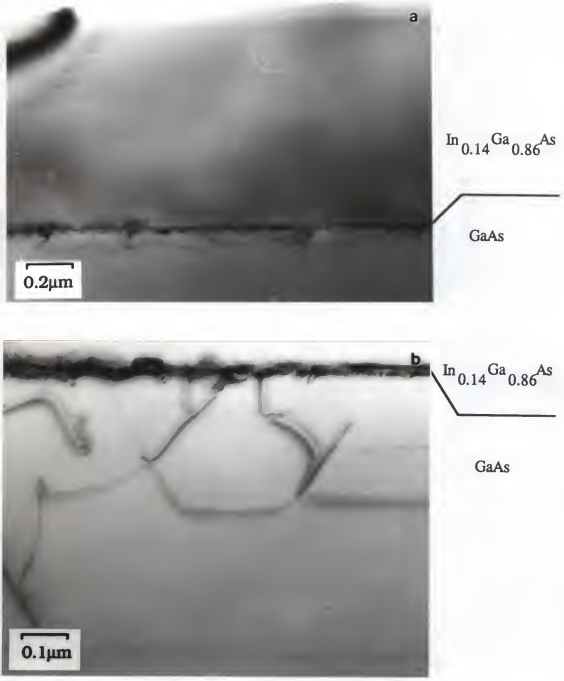

Figure 3-1. Cross-sectional TEM micrographs of an $In_{0.14}Ga_{0.86}As$/GaAs heterostructure.
a) A micrograph showing the absence of dislocations in the epilayer; b) Dislocations in the GaAs substrate.

dark band to be a result of the strain field from misfit dislocations at the heterointerface. The discrete misfit dislocations can be clearly seen in the XTEM micrograph of Figure 3-2 obtained from a specimen that was severely tilted off the (011) zone.

Cross-sectional TEM analysis of medium x structures indicated the presence of threading dislocations in the epilayer as well as dislocations in the GaAs substrate and the heterointerface as shown in Figures 3-3a and 3-3b. Analysis of large x ($x>0.4$) $In_xGa_{1-x}As/GaAs$ structures showed the presence of threading dislocations in the $In_xGa_{1-x}As$ epilayer and an absence of dislocations in the GaAs substrate as shown in Figures 3-4a and 3-4b.

Planar TEM analysis was performed on small and large x structures to determine threading dislocation densities in such epilayers and a comparison of the dislocation structure in a $In_{0.14}Ga_{0.86}As$ (small x) layer versus that in a $In_{0.4}Ga_{0.6}As$ (large x) layer is shown in Figure 3-5. The threading dislocation density in the $In_{0.4}Ga_{0.6}As$ epilayer was about $10^{10}/cm^2$. Since the PTEM specimen of the $In_{0.14}Ga_{0.86}As$ epilayer showed the absence of threading dislocations, an estimate of the threading dislocation density using this technique was not possible. The etch-pit technique was therefore required to determine the threading dislocation density in such small x layers. A scanning electron micrograph of an etched specimen is shown in Figure 3-6. The calculated threading dislocation density in the $In_{0.14}Ga_{0.86}As$ epilayer was about $10^4/cm^2$.

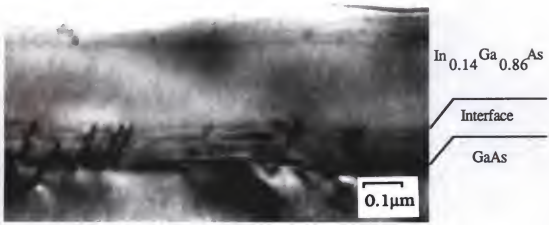

Figure 3-2. Transmission electron micrograph of a severely tilted heterointerface showing discrete misfit dislocations.

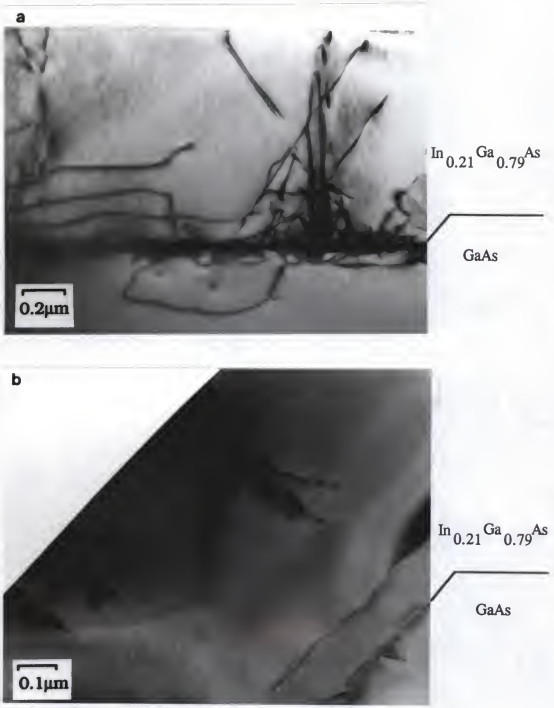

Figure 3-3. Cross-sectional TEM micrographs of a medium x $In_{0.21}Ga_{0.79}As$ layer showing dislocation formation in both the epilayer and the substrate.
a) Low magnification and b) High magnification.

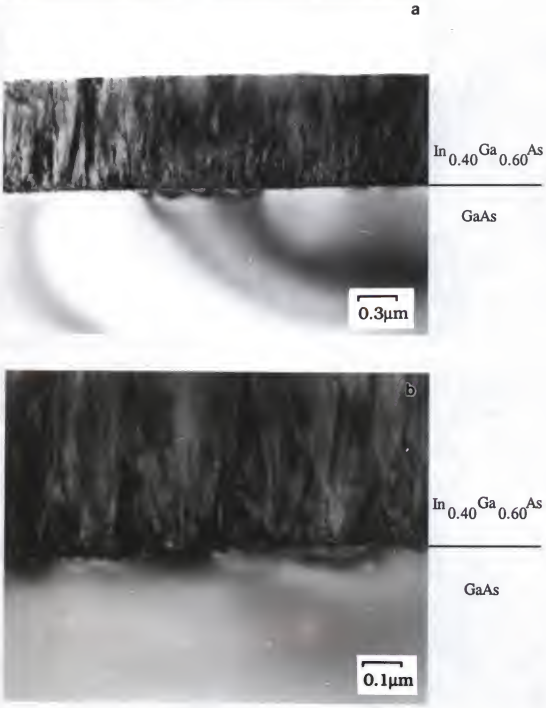

Figure 3.4: Cross sectional TEM micrograph of a large x $In_{0.4}Ga_{0.6}As$ layer.
a) Micrograph showing extensive dislocation formation in the epilayer; b) Micrograph showing a lack of dislocations in the substrate.

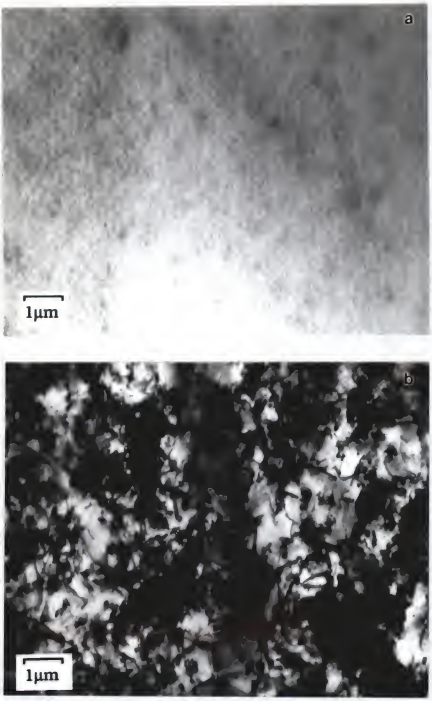

Figure 3.5: Plan view TEM micrographs of small and large x layers. a) Micrograph of an $In_{0.14}Ga_{0.86}As$ layer showing a lack of dislocations; b) Micrograph of a $In_{0.4}Ga_{0.6}As$ layer showing an extensive network of dislocations.

3.3 Discussion of Results

The observation of dislocations in the GaAs substrate in small x ($x<0.18$) $In_xGa_{1-x}As$/GaAs single-layer structures is consistent with a previously reported study of Fitzgerald et al. [28] which specifically concerned $In_{0.12}Ga_{0.88}As$/GaAs samples. The force acting on dislocations which promotes movement into the GaAs material is a repulsive force due to dislocations having the same Burgers vector at the $In_xGa_{1-x}As$/GaAs interface while the major opposing force attracting dislocations back to the heterointerface is an interface image force. Thus a balance of forces would cause the formation of bowed dislocations or dislocation half-loops in the GaAs material. Such bowed dislocations seemed to be present in the small x structures as shown in Figures 3-1a and 3-1b. However, as noted in chapter 2, the absence of threading dislocations in the $In_xGa_{1-x}As$ epilayers (small x) was not well explained by Fitzgerald et al. [28] who reasoned that the larger misfit stress in the epilayer leads to the absence of threading dislocations. However, such a larger misfit stress in the epilayer is common to other lattice-mismatched systems where an absence of threading dislocations in the epilayer is not observed.

The absence of threading dislocations in the epilayer of epilayer/substrate lattice-mismatched systems is unique to the $In_xGa_{1-x}As$/GaAs material system for small values of x. This unique trait can be explained on the basis of a comparison of the high temperature mechanical properties of $In_xGa_{1-x}As$ versus those of GaAs. At room temperature $In_xGa_{1-x}As$ is softer (or has a lower yield strength) than GaAs [1]. However, compression tests and hardness studies conducted

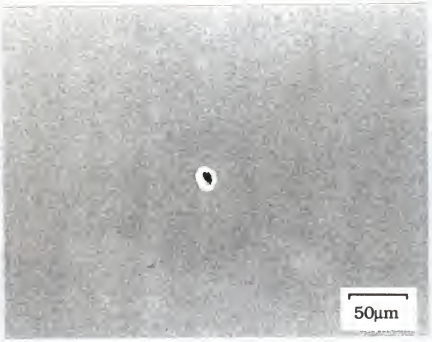

Figure 3-6. Scanning electron micrograph of an etch-pit in a $In_{0.14}Ga_{0.86}As$ epilayer. Using several such micrographs, the dislocation density was determined to be $10^4/cm^2$.

by Bourret et al. [55-57] on In doped GaAs (x=0.001) show that in comparison to GaAs, the yield strength of the In doped material decreases more gradually with increase in temperature. The results also show that a critical temperature exists at which the yield strengths of In doped and undoped GaAs material are identical, the critical temperature being found to be 390°C. At temperatures greater than the critical temperature, the In doped alloy has a greater yield strength than that of the undoped GaAs material and for temperatures lower than the critical temperature, undoped GaAs has a greater yield strength than In doped GaAs. Also, high temperature (780°C) compression tests conducted by Djemel and Castaing [58] on In doped GaAs material (x=0.004) and undoped GaAs show that the yield strength of the doped GaAs material is about three times greater than that of undoped GaAs.

Ehrenreich and Hirth [59] have speculated that the increase in high temperature yield strength of GaAs upon In doping is due to solid solution hardening. In the case of metals, single solute atoms can produce solution hardening [60]. For GaAs, by contrast, the corresponding solute entity consists of 5-atom clusters surrounded by anions. The presence of a single 5-atom $InAs_4$ unit in GaAs leads to a local bond extension of about 7% (equal to the lattice parameter difference between InAs and GaAs) or equivalently a volume dilation of 21%. Therefore, this unit can act as a strain center and should result in substantial solid solution strengthening. The assumption that the $InAs_4$ unit causes all of the observed dilation is reasonable since composition dependence studies of the bond lengths on $In_xGa_{1-x}As$ alloys [61] show that the As sublattice, while retaining a tetrahedral

configuration, distorts appreciably in such a way that the As neighbors surrounding the Ga atoms contract while those surrounding In atoms expand, allowing a volumetric difference of 21% between an $InAs_4$ unit and its surrounding $GaAs_4$ units.

Guruswamy et al. [62] conducted high temperature (25-900°C) hardness tests on In doped GaAs alloys (x=0.0025 and 0.01) and found that the high temperature hardness of the $In_{0.01}Ga_{0.99}As$ alloy is greater than that of the $In_{0.0025}Ga_{0.9975}As$ alloy. Since the hardness can be related to the yield stress, it was determined that the yield stress of the $In_{0.01}Ga_{0.99}As$ alloy is greater than that of the $In_{0.0025}Ga_{0.9975}As$ alloy showing an increasing trend in the yield strength with increasing x value. Guruswamy et al. [62] noted a soft-hard transition with increasing temperature for the In doped alloys in comparison to undoped GaAs but could not obtain an exact value for the transition temperature due to the scatter in the hardness data. These authors speculated that the transition could be explained based on the action of two opposing mechanisms, a rate-controlling mechanism related to the intrinsic lattice resistance or Peierl's barrier versus a mechanism for dislocation propagation. At low temperatures, the Peierl's barrier mechanism is operative and thus the addition of In could soften the GaAs material. However, as the temperature is increased, the hardness of the alloy is determined by the resistance to dislocation glide by solute atoms or $InAs_4$ units and thus the addition of In increases the high temperature hardness of GaAs.

In the case of small x $In_xGa_{1-x}As$ layers grown on GaAs, the smaller yield strength of GaAs at the growth temperature allows the

GaAs substrate to yield prior to the $In_xGa_{1-x}As$ epilayer upon application of strain (such as lattice-mismatch strain in the $In_xGa_{1-x}As$/GaAs system) and hence the observation of dislocations in the GaAs substrate and a lack of dislocations in the $In_xGa_{1-x}As$ epilayer. The propagation of dislocations into the GaAs partially relieves strain in addition to the formation of misfit dislocations at the heterointerface. Also, the absence of dislocations in the epilayer suggests dislocation nucleation at the heterointerface.

There are several possible theories that need to be explored in order to explain the evolution of dislocations in medium and large x $In_xGa_{1-x}As$/GaAs structures. Based on the argument presented above for small x $In_xGa_{1-x}As$/GaAs structures, i.e. that of solid solution hardening, one could attempt to explain the presence of dislocations in medium and large x $In_xGa_{1-x}As$ layers.

It is possible, for instance, that the solid solution hardening effect due to In addition may have peaked at an $In_xGa_{1-x}As$ composition of x=0.18. This peak would explain the presence of threading dislocations in the $In_xGa_{1-x}As$ material since for $In_xGa_{1-x}As$/GaAs structures with $x>0.18$, the yield strength of the $In_xGa_{1-x}As$ epilayer would be less than that of GaAs allowing the epilayer to yield prior to the GaAs substrate. However, the presence of dislocations in the GaAs substrate in medium x structures suggests that the substrate has a comparable yield strength to that of the epilayer at the corresponding growth temperature. This does not seem possible since the presence of dislocations in both the substrate and epilayer occurs over a broad range of compositions, i.e. $0.18<x<0.28$. In actual fact, as will be seen in chapter 5, based on the

analysis of multilayer structures, the yield strength of $In_xGa_{1-x}As$ appears to continually increase up to an x value of ~0.5 at elevated temperatures.

A second possible explanation for the presence of threading dislocations in medium and large x $In_xGa_{1-x}As$ epilayers could involve a planar (two-dimensional) to island (three-dimensional) growth mode transition at $In_xGa_{1-x}As$ epilayer compositions ≥0.18. In this case, during growth, the $In_xGa_{1-x}As$ epilayer would be deposited in the form of discrete islands which would grow laterally and coalesce giving rise to threading dislocations at the imperfect island junctions. Three-dimensional growth (island growth) can be observed, in-situ, by analytical tools such as reflection high energy electron diffraction (RHEED) wherein a streaky pattern would signify a smooth surface or planar growth and a spotty pattern would represent a rough surface as in the case of island growth. However, RHEED analyses on $In_xGa_{1-x}As$/GaAs epilayers performed by several research groups [35-37] have shown that planar growth is sustained up to $In_xGa_{1-x}As$ compositions ~0.5. Also the growth conditions employed in this work (as mentioned in Chapter 2) were optimized such that the RHEED patterns remained streaky during growth. Furthermore, a 2D to 3D growth mode transition cannot explain the presence of dislocations in the GaAs substrate in the medium x $In_xGa_{1-x}As$/GaAs structures. Therefore, the mechanism of 2D-3D growth mode transition cannot be utilized to explain dislocation evolution in medium and large x $In_xGa_{1-x}As$/GaAs structures.

A third possible mechanism by which threading dislocation evolution in $In_xGa_{1-x}As$ epilayers could be explained would be that of

surface nucleation of dislocations. However, as indicated in the XTEM micrographs of small x structures, nucleation of dislocations seems to occur at the $In_xGa_{1-x}As/GaAs$ heterointerface, suggesting that interface nucleation is energetically favourable when compared to surface nucleation. Therefore, one can assume that the first dislocations to form in medium x $In_xGa_{1-x}As$ structures would nucleate at the heterointerface when the critical thickness is reached. These dislocations would relieve strain in the epilayer as they extend across the interface. Consequently, it is difficult to envision surface nucleation of dislocations given the larger amount of energy required to nucleate such dislocations.

In the following section a theory based on a balance of forces acting on a dislocation near the heterointerface is proposed in order to explain the observed dislocation evolution as a function of composition in the $In_xGa_{1-x}As/GaAs$ material system.

3.4 A Force Balance Mechanism for Dislocation Evolution

As mentioned previously, it is well known that strain relief occurs by the formation of misfit dislocations above a critical thickness and that the critical thickness decreases with increasing lattice-mismatch strain. In the previous section it was shown that the presence of dislocations in the substrate material as opposed to the epilayer can only be explained on the basis of dislocation nucleation at the heterointerface. Therefore, at the onset of strain relief, i.e. at the

critical thickness, one can assume that misfit dislocations have already nucleated and are lying in the plane of the $In_xGa_{1-x}As/GaAs$ interface. The force balance mechanism to be discussed below will only be applicable in the case where the epilayer is harder than the substrate at the growth temperature since, if the converse were true, surface nucleation of dislocations would become a viable option.

In general terms, several forces act on a misfit dislocation segment that begins to propagate into an epilayer and, depending on the net force, such a segment may either further propagate into the epilayer or may retract towards the heterointerface. Similarly, specific forces act on dislocations that may propagate into the substrate.

A dislocation on the epilayer side of the heterointerface would experience a surface image force due to its proximity to the free surface. The surface image force (F_{se}) would attract the dislocation towards the free surface and can be represented as

$$F_{se} = \frac{G_e b^2 (1 - \nu\cos^2\beta)}{4\pi(1 - \nu)d}$$

where G_e is the shear modulus of the epilayer material, d is the thickness of the epilayer, b is the Burgers vector, ν is the Poisson's ratio and β is the angle between the dislocation direction and the Burgers vector. A second force that would move the dislocation towards the surface would be a repulsive force (F_{de}) from dislocations at the interface that have the same Burgers vector and is given by [28]

$$F_{de} = \left(\frac{G_e b_e^2}{2\pi(1 - \nu)}\right) \sum \frac{x(x^2 - y^2)}{(x^2 + y^2)^2} + \left(\frac{G_e b_s^2}{2\pi}\right) \sum \frac{x}{(x^2 + y^2)}$$

where the first term represents the force from the edge component along the <111> direction (x direction) and the second term represents the screw component resolved along x, b_e and b_s are the edge and screw components of the Burgers vector and the summation is over dislocations at the interface.

The major force that prevents the motion of dislocations towards the surface is the force from the elastic strain in the epilayer given by

$$F_{ee} = \left(\frac{a}{2\sqrt{3}}\right)\frac{G_e\varepsilon}{(1-\nu)}$$

where ε is the misfit strain in the epilayer and a is the lattice parameter of the epilayer. Other forces that prevent the motion of dislocations towards the surface include the Peierls force (F_{pe}), an interface image force (F_{ie}) and a line tension force (F_{le}) which are given by [63]

$$F_{pe} = \frac{2G_eb^2}{(1-\nu)}\exp -\left(\frac{2\pi d}{(1-\nu)b}\right)$$

where d is the interplanar spacing between (110) planes,

$$F_{le} = \left[\frac{G_eb^2}{4\pi(1-\nu)}\right]\left[\frac{(1-\nu\cos^2\beta)\sin\theta}{R}\right]$$

where θ is the angle between the slip plane and the interface plane and R is the cutoff radius of the dislocation which is typically taken as the distance to the interface thus making the expression inaccurate when near the interface and

$$F_{le} = \alpha\left(\frac{G_e b^2}{4\pi\,(1-\nu)}\right)\frac{(1-\nu\cos^2\beta)}{\rho}\left[\ln\left(\frac{x\sin\theta}{b}\right)+2\right]$$

where α is a constant based on the geometry of the dislocation segment and ρ is the radius of curvature of the segment.

A dislocation in the GaAs substrate would experience all of the aforementioned forces with the exception of the surface image force [28]. Also, all of the forces are strongly dependent on the shear modulus of the material at the growth temperature [62] and hence, these forces will be weaker in the GaAs than in the epilayer material. Since the substrate is much thicker than the epilayer material, most of the elastic strain should reside in the epilayer material. Hence, the force from the elastic strain would be much greater in the epilayer than in the substrate. The net force acting on a dislocation in the $In_xGa_{1-x}As$ epilayer allowing it to move towards the free surface can be expressed as

$$F_{epi} = F_{se} + F_{de} - F_{pe} - F_{ee} - F_{ie} - F_{le}$$

while the net force acting on a dislocation in the GaAs allowing it to traverse further into the substrate is given by

$$F_{sub} = F_{ds} - F_{ps} - F_{es} - F_{is} - F_{ls}$$

where the subscript s stands for the force acting on a dislocation in the GaAs. Of the various forces acting on a dislocation, the surface image force and the elastic strain force are the ones that are extremely dependent on $In_xGa_{1-x}As$ composition. As the composition of $In_xGa_{1-x}As$, i.e. the x value, increases, the critical thickness

decreases due to the increasing lattice-mismatch strain. Therefore, the surface image force increases with increasing $In_xGa_{1-x}As$ composition. However, the major force that prevents a dislocation from traversing to the surface, i.e. the elastic strain force (F_{ee}), also increases with increasing $In_xGa_{1-x}As$ composition. A ratio of the surface image force to the elastic strain force as a function of epilayer composition, x, is plotted in Figure 3-7. The critical thicknesses used to calculate the surface image force values were obtained from Matthews equation to predict the critical thickness given by

$$h_c = \frac{b}{8\pi\varepsilon(1+\nu)}\left[1 + \ln\left(\frac{h_c}{b}\right)\right]$$

where ε is the misfit strain. The plot in Figure 3-7 indicates that for small x structures, the surface image force is small due to the large values of critical thickness. Also, since $F_{ee} \gg F_{es}$, F_{epi} is much smaller than F_{sub}. Therefore, dislocations in the small x structures should appear only in the GaAs as, in fact, has been observed. At some "critical composition" the surface image force would become comparable to the elastic strain force, thus allowing dislocations to traverse to the free surface. This composition, as narrowed down by XTEM analysis, appears to be at $x \approx 0.18$.

In medium x structures, F_{se} becomes significantly larger and hence F_{epi} can approximate F_{sub}. Thus, the observation of dislocations in both the epilayer and the GaAs in this case. Finally, for very large values of F_{se}, as in the case of large x structures, F_{epi} will become much greater than F_{sub} and hence all of the dislocations will

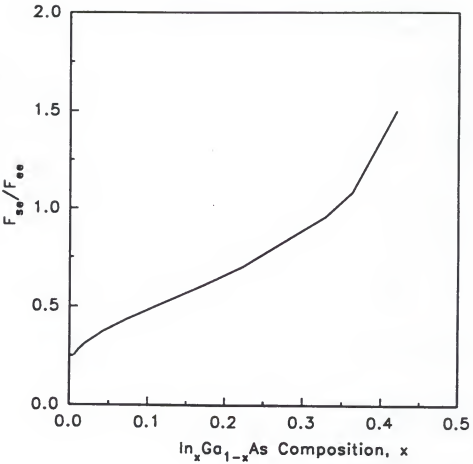

Figure 3-7. A plot of the ratio of the surface image force (Fse) to the misfit force (Fee) versus $In_xGa_{1-x}As$ composition showing an increase in the surface image force with increasing composition.

be able to travel to the free surface leaving the GaAs dislocation free as observed in this work.

3.5 Summary

In summary, it has been shown that a "critical composition" of $x \approx 0.18$ exists in the $In_xGa_{1-x}As/GaAs$ system up to which $In_xGa_{1-x}As$ layers can be grown directly on GaAs without the evolution of threading dislocations in the epilayer. This trait of the $In_xGa_{1-x}As/GaAs$ material system has been explained by assuming that $In_xGa_{1-x}As$ has a greater yield strength than that of GaAs at the growth temperature which causes the substrate to yield preferentially and hence relax the misfit strain. Also, dislocation evolution in the $In_xGa_{1-x}As/GaAs$ system as a function of x has been explained by assuming that a balance of forces acting on misfit dislocations near the heterointerface is attained. The magnitude of the various forces, which are very much alloy composition dependent, determine whether or not dislocations propagate in the epilayer or the substrate, or indeed, both the epilayer and the substrate.

CHAPTER 4
STRAIN RELIEF IN $In_xGa_{1-x}As$-BASED STRAINED LAYER SUPERLATTICE SYSTEMS

4.1 Introduction

In the previous chapter it was shown that low-dislocation density ($10^4/cm^2$) $In_xGa_{1-x}As$/GaAs epilayers can be grown directly on GaAs for x values ≤ 0.18. However, epilayers having x values greater than 0.18 were shown to contain a high density of threading dislocations. The work to be described in the following chapter concerned the use of $In_xGa_{1-x}As$-based strained layer superlattices (SLSs) which were investigated with a view towards reducing the threading dislocation density in $In_xGa_{1-x}As$/GaAs epilayers having x values greater than 0.18.

4.2 Single Strained Layer Superlattice Buffer Structures

As discussed in the literature review section, strained layer superlattices have been shown to be somewhat effective in blocking dislocations from propagating into epilayers in lattice-mismatched systems in which case dislocation bending by strain fields appears to be the primary factor responsible for dislocation blocking..

In order to determine the effectiveness of such SLSs in terms of reducing the dislocation density, for example, in an $In_{0.4}Ga_{0.6}As$/ GaAs epilayer, a SLS consisting of 100 periods of 10Å thick alternate layers of GaAs and $In_{0.8}Ga_{0.2}As$ was grown on GaAs and a 1μm thick $In_{0.4}Ga_{0.6}As$ layer was grown on the SLS. The x=0.8 composition was chosen in this case in order that the average composition of the SLS match that of the epilayer. XTEM analysis of the structure showed that dislocations which formed at the GaAs/SLS heterointerface threaded through the SLS and the $In_xGa_{1-x}As$ epilayer to the free surface (Figure 4-1). It was therefore concluded that this particular SLS was ineffective as a dislocation blocker. The ineffectiveness of the SLS could be due to the large lattice-mismatch strain of 3% between substrate and SLS and/or the large mismatch strain of 6% between the individual layers in the SLS. In a second experiment, a single $In_{0.3}Ga_{0.7}As$/ $In_{0.5}Ga_{0.5}As$ SLS was grown directly on GaAs so that the mismatch between individual layers in the SLS would be significantly reduced when compared to the previously studied SLS, while the mismatch between the substrate and SLS would be the same as in the previous case (3%). The thickness of individual layers was maintained below the critical thickness at a value of 100Å and a 1μm thick $In_{0.4}Ga_{0.6}As$ layer was grown on top of the SLS. XTEM analysis of the heterostructure showed dislocations propagating through the superlattice to the top $In_{0.4}Ga_{0.6}As$ layer (Figure 4-2a). A closer observation of the SLS (Figure 4-2b) indicated that the dislocations were not at all bent by the stresses within the individual SLS layers. The ineffectiveness of such SLSs was attributed to the large mismatch strain existing between the substrate and the SLS and, in order to

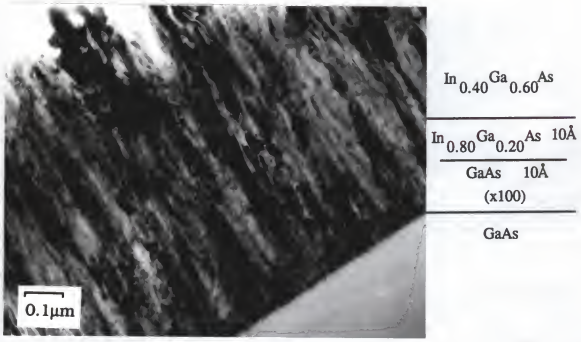

Figure 4-1. Cross-sectional TEM micrograph showing a single SLS incorporated between the GaAs substrate and an $In_{0.4}Ga_{0.6}As$ layer. The SLS is not resolved due to the extremely small thicknesses of individual layers. Extensive threading dislocation formation is noticed in the epilayer.

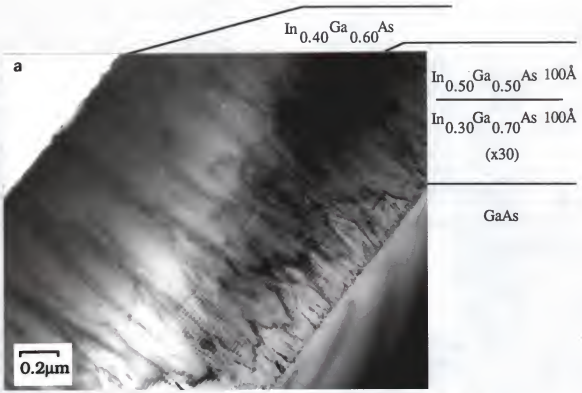

Figure 4-2. Cross-sectional TEM micrographs of a single SLS structure designed to block dislocations.
a) Micrograph of the entire structure; b) High-magnification of the SLS showing its ineffectiveness in blocking dislocations.

achieve low dislocation density large x $In_xGa_{1-x}As$ layers, it was decided that perhaps a multistage buffer system would be necessary wherein strain relief would occur on a gradual basis upon growth of each stage. In the following section the design and analysis of such a strain relief structure is detailed.

4.3 Design and Analysis of Multistage Strain Relief Systems Containing Strained Layer Superlattices

The buffer system in this work comprised stacked stages which were designed in such a way as to promote strain relief and dislocation blocking in underlying layers of the stack leaving the top layer relatively dislocation-free. XTEM analysis was conducted after each stage of the stacked structure was grown and design of each subsequent stage was based on this analysis. The additional stage was incorporated in the multistage heterostructure which was then grown anew.

A 0.2μm thick $In_{0.14}Ga_{0.86}As$ layer was chosen for the first stage of the multistage system since such a composition lies below the critical composition of x=0.18. Strain relief at this stage occurs by the evolution of dislocations at the $In_{0.14}Ga_{0.86}As/GaAs$ heterointerface and in the GaAs substrate as explained in the previous chapter.

A 0.2μm thick $In_{0.27}Ga_{0.73}As$ layer was grown at the second stage so that the difference in compositions between the first and second stages would be below the critical composition. However, XTEM analysis of the two-stage system revealed a high density of threading dislocations in the top layer (Figure 4-3). At this point it

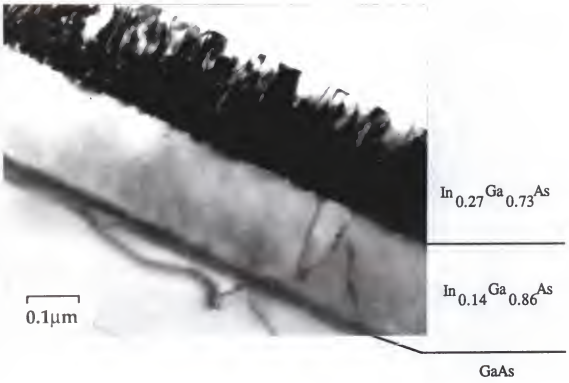

Figure 4-3. Cross-sectional TEM micrograph of a two-layer structure showing extensive threading dislocation generation in the top $In_{0.27}Ga_{0.73}As$ layer.

was decided that a SLS would be necessary between the $In_{0.14}Ga_{0.86}As$ and $In_{0.27}Ga_{0.73}As$ layers to block dislocations from propagating into the top layer. The compositions of the alternating layers in the SLS were chosen to be x=0.14 and x=0.4 such that the average composition of the SLS would equal the top layer composition. The thicknesses of the layers were chosen to be 20Å which is less than the critical thickness and therefore dislocation nucleation within the SLS structure would not be a concern. An XTEM micrograph of the two stage structure consisting of a single $In_xGa_{1-x}As$ layer at stage 1 and a 50 period SLS at stage 2 is shown in Figure 4-4a. As can be seen from the figure, dislocation formation in the $In_{0.14}Ga_{0.86}As$ layer is evident along with the presence of a few dislocations in the SLS. Dislocations in the SLS appeared to be effectively bent by the stresses present in the SLS layers as evidenced by the lack of dislocations in the layers near the surface. A 0.2μm $In_{0.27}Ga_{0.73}As$ layer was chosen for the third stage since it should be lattice-matched to the underlying SLS. XTEM analysis of the three-stage structure showed a lack of threading dislocations in the top layer (Figure 4-4b). A comparison of this three-stage structure to the structure shown in Figure 4-3 clearly shows the advantage of using a SLS to block dislocations. HRXRD analysis was performed to study lattice-matching between the second and third stages of the structure shown in Figure 4-4. Typical rocking curves at a (444) reflection obtained from two- and three-stage structures (Figure 4-5) indicated two epilayer peaks for both structures. In the two-stage structure these two epilayer peaks correspond to stages 1 and 2 of the heterostructure, respectively. The peak representing the SLS at stage 2 corresponds

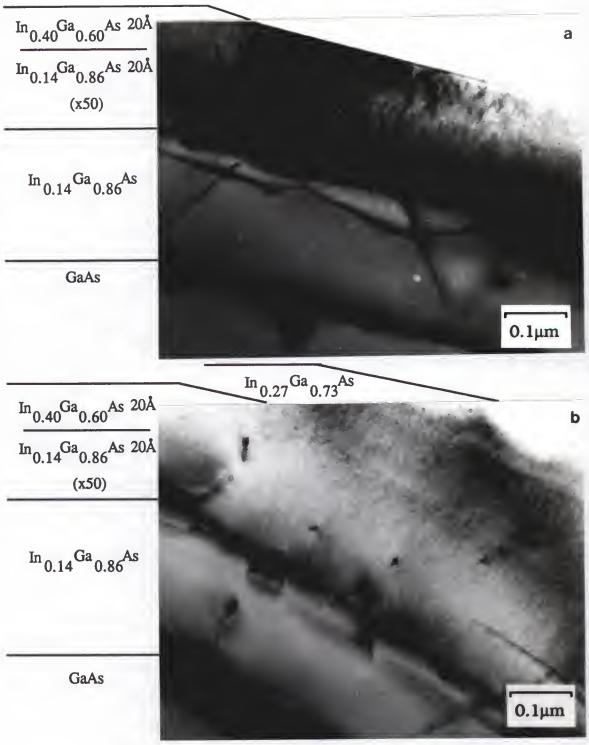

Figure 4-4. Cross-sectional TEM micrographs of two- and three-stage structures showing effective dislocation blocking by the SLS at stage 2 resulting in a low dislocation density $In_{0.27}Ga_{0.73}As$ layer.
a) Two-stage structure; b) Three-stage structure.

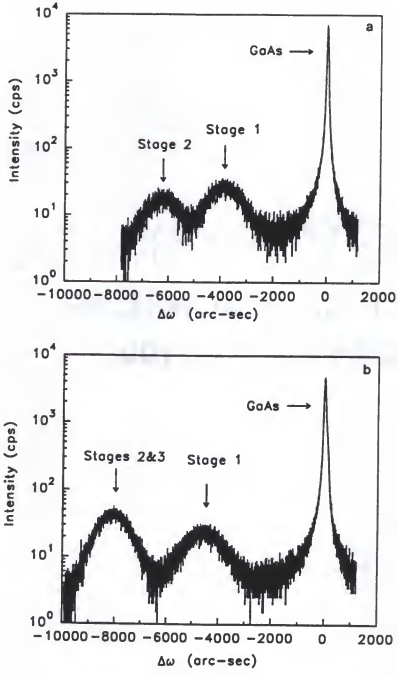

Figure 4-5. X-ray rocking curves obtained from the ω^- condition of (444) planes.
a) Rocking curve from a two-stage structure; b) Rocking curve from a three-stage structure showing an overlap of peaks from stages 2 and 3.

to its 0th order peak. Higher order, or satellite, peaks are not seen in the rocking curve shown in Figure 4-5a due to the limited angular scan range ($\Delta\omega$) employed. A HRXRD analysis of the three-stage structure revealed that stages 2 and 3 are represented by a single epilayer peak (Figure 4-5b). Therefore, one can conclude that the two stages are lattice-matched in both the in-plane, or parallel, and perpendicular directions.

A second SLS was chosen for use at the fourth stage of the multistage structure and designed such that the difference between the average composition of the SLS and that of the underlying layer (x=0.27) was below the critical composition of x=0.18. The compositions of the individual $In_xGa_{1-x}As$ layers comprising the SLS were chosen to be x=0.27 and x=0.53, respectively, giving an average SLS composition of x=0.4. The thicknesses of the individual layers were 20Å each and there were 50 periods forming the SLS. XTEM analysis of the four-stage structure showed dislocation evolution in the underlying third stage (Figure 4-6a). Dislocations were also observed in the SLS grown at the fourth stage. Most of the dislocations in the SLS seemed to be blocked and diverted toward the edges of the specimen. However, a few dislocations appeared to traverse through the SLS to the free surface. These dislocations appeared to be nucleating within the SLS rather than at the Stage 3/ Stage 4 interface. Since the mismatch between alternating layers in the SLSs at both stages 2 and 4 are equal (lattice parameter difference, Δa, is constant since compositional difference, Δx, is constant at a value Δx=0.26), the nucleation of dislocations or yielding within the SLS at stage 4 could be explained assuming that the yield strength of one of

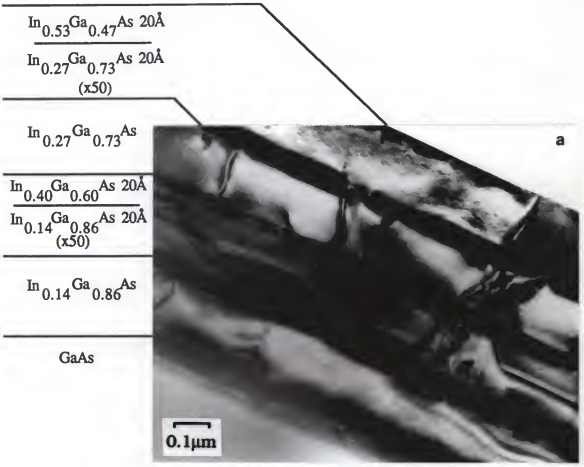

Figure 4-6. Cross-sectional TEM micrographs of four- and five-stage structures.
a) Micrograph of a four-stage structure showing strain relief in stages 1-3. The fourth stage SLS shows a few dislocations that appear to propagate to the free surface.

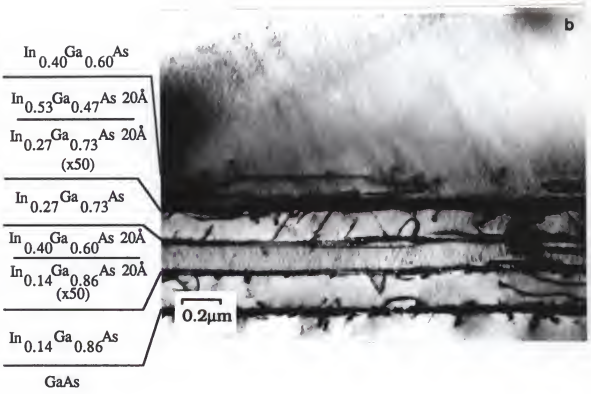

Figure 4-6--continued
b) Micrograph of a five-stage structure showing a lack of dislocations in the top $In_{0.4}Ga_{0.6}As$ layer.

the layers in the SLS is smaller than that of the single $In_xGa_{1-x}As$ layer at stage 3. The yield strength as a function of $In_xGa_{1-x}As$ composition will be discussed in greater detail in Chapter 5.

A 1μm thick single $In_xGa_{1-x}As$ layer with a composition of x=0.4 was chosen for the fifth stage due to its match to the average lattice parameter of the SLS at stage 4. XTEM analysis of the structure revealed that the top $In_xGa_{1-x}As$ layer was relatively dislocation-free (Figure 4-6b) while strain relaxation occurred by dislocation evolution in the underlying stages, i.e. stages 1-4. HRXRD analyses of four- and five-stage structures showed the presence of four epilayer peaks in the respective x-ray rocking curves (Figure 4-7). The presence of four epilayer peaks corresponding to the four stages in the four-stage structure (Figure 4-7a) suggests that the superlattice at stage 2 relaxed to a different extent when compared to the single $In_xGa_{1-x}As$ layer at stage 3 upon growth of the fourth stage, since, prior to the growth of the fourth stage, stages 2 and 3 were lattice-matched (Figure 4-5b). Such a relaxation difference between stages 2 and 3 can be expected since the SLS is made up of two different layers (in terms of composition) whose mechanical properties are very different. Therefore, one half of the SLS could yield at a vastly different rate in comparison to the other half and consequently, the net strain relaxation of the SLS would be different when compared to that of the single layer stage whose composition and hence properties are different from those of the layers in the SLS.

Plan-view TEM analysis of the five-stage structure (Figure 4-8) revealed that the threading dislocation density in the $In_{0.4}Ga_{0.6}As$ top layer was about $10^6/cm^2$. Such a defect density has proved to be

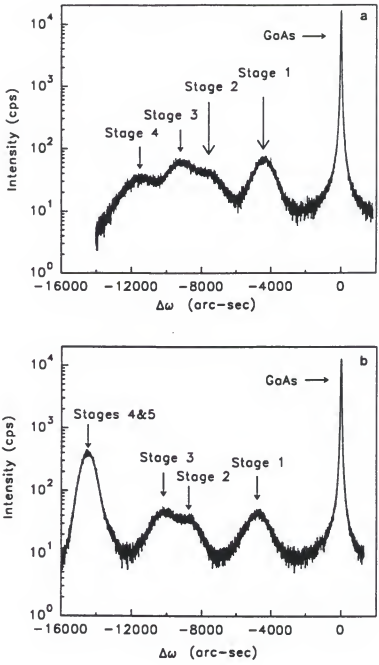

Figure 4-7. X-ray rocking curves obtained using the ω^- condition on (444) planes.
a) Rocking curve from a four-stage structure showing discreet peaks representing stages 2 and 3, respectively;
b) Rocking curve from a five-stage structure showing an overlap of peaks representing stages 4 and 5.

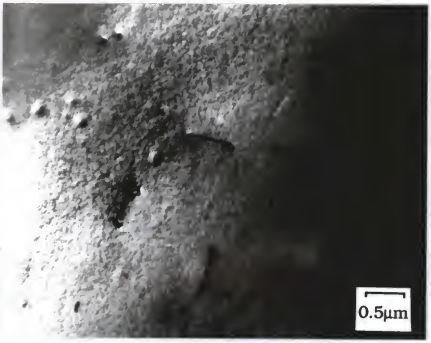

Figure 4-8. Plan-view TEM micrograph of the $In_{0.4}Ga_{0.6}As$ top layer showing a few threading dislocations. The dislocation density was determined as being $10^6/cm^2$.

sufficiently low for the production of good quality $In_{0.4}Ga_{0.6}As/GaAs$ photodetectors [64]. However, a much lower dislocation density ($<10^5/cm^2$) would probably be required for the production of more defect sensitive devices such as LEDs and diode lasers. A close examination of the stage 4 superlattice in the five-stage structure (Figure 4-9) showed that some dislocations were unaffected by the superlattice and were able to traverse to the top layer thus contributing to the threading dislocation density observed by PTEM. In an effort to design more effective dislocation-blocking SLSs, the thicknesses of the individual layers in the SLS at the fourth stage was altered to 10Å, 50Å and 100Å in three separately grown five-stage structures so that the stresses in the SLS layers would be different. The compositions of the individual layers comprising the SLS and the total number of periods were maintained the same as before. XTEM analysis of the SLSs indicated no change with regard to the effectiveness of the various superlattices in blocking dislocations.

In order to study the compositional range over which such low dislocation density $In_xGa_{1-x}As$ layers could be obtained by the use of the multistage strain relief buffer system, a seven-stage structure was designed wherein the sixth stage consisted of a SLS and the seventh stage consisted of a 1μm thick $In_{0.48}Ga_{0.52}As$ layer that was lattice-matched to the underlying superlattice. The SLS comprised 50 periods of 20Å thick alternating $In_{0.4}Ga_{0.6}As$ and $In_{0.56}Ga_{0.44}As$ layers. XTEM analysis of the seven-stage structure showed extensive threading dislocation evolution in the top $In_{0.48}Ga_{0.52}As$ layer (Figure 4-10). PTEM analysis of the top layer revealed that the threading dislocation density was about $10^8/cm^2$ (Figure 4-11).

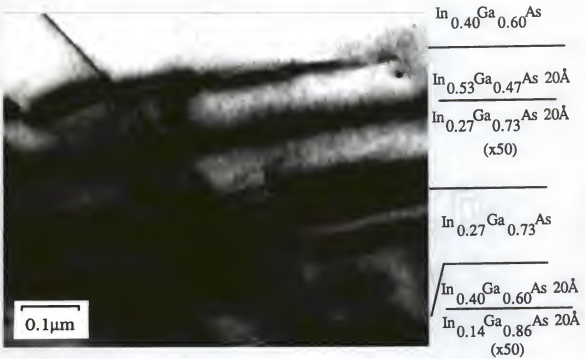

Figure 4-9. Cross-sectional TEM micrograph of the fourth stage SLS in the five-stage structure showing a dislocation propagating through the superlattice to the top layer without being affected by the stresses in the SLS.

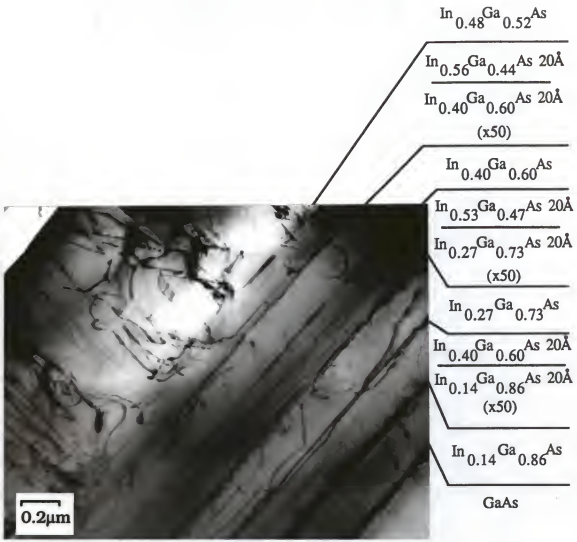

Figure 4-10. Cross-sectional TEM micrograph of a seven-stage structure showing extensive threading dislocation formation in the top $In_{0.48}Ga_{0.52}As$ layer.

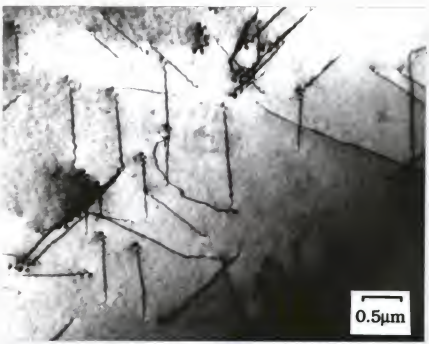

Figure 4-11. Plan-view TEM micrograph of a $In_{0.48}Ga_{0.52}As$ top layer showing a high density of threading dislocations despite the use of a strain relief buffer.

4.4 Summary and Conclusions

A multistage strain relief buffer structure involving several SLSs as opposed to a single SLS was shown to be fairly effective in terms of reducing the density of dislocations threading in $In_xGa_{1-x}As$ layers having x values >0.18. The smallest dislocation density obtained by use of a multistage buffer in the case of $In_{0.4}Ga_{0.6}As$ material was $\sim 10^6/cm^2$. However, attempts at further dislocation density reduction by varying the SLS structure proved unsuccessful, which was probably due to dislocation generation within the SLSs themselves. In terms of growing relatively low dislocation density $In_xGa_{1-x}As$ on GaAs employing SLSs, a maximum $In_xGa_{1-x}As$ composition of $x \approx 0.4$ was determined. Clearly, a different method of accomodating strain relief would be necessary to provide low dislocation density large x $In_xGa_{1-x}As$ epilayers on GaAs.

CHAPTER 5
STRAIN RELIEF IN STACKED $In_xGa_{1-x}As$ MULTILAYER SYSTEMS NOT INVOLVING STRAINED LAYER SUPERLATTICES

5.1 Introduction

As concluded in the previous chapter, a strain relief system other than one involving SLSs would be required in order to extend the composition range over which low-dislocation density ($<10^5/cm^2$) $In_xGa_{1-x}As$ could be grown. With such an objective in mind, it was decided that in order to effectively utilize the strain relief mechanism proposed in chapter 3 toward the development of multilayer $In_xGa_{1-x}As$ structures, a quantitative understanding of the extent of strain relaxation occurring in each layer of a multilayer system would be vital. To this end, the extent of lattice relaxation occurring in single $In_xGa_{1-x}As/GaAs$ heterostructures as functions of composition and layer thickness was first of all studied and the results of this work are detailed in section 5.2 below. This work was then extended to stacked multilayer $In_xGa_{1-x}As$ systems, the extent of lattice relaxation occurring in each layer of a stacked system being determined as a function of the number of layers forming the stacked structures.

5.2 Extent of Residual Strain in Single $In_xGa_{1-x}As/GaAs$ Heterostructures

In order to study the extent of strain relaxation in single $In_xGa_{1-x}As$ layers grown on GaAs, a variety of layers were grown having various compositions (as determined by electron microprobe analysis) and thicknesses and high resolution x-ray diffraction (HRXRD) analysis was performed on the samples. All of the x-ray rocking curves were obtained after optimizing the tilt of the specimen for maximum substrate peak intensity as explained in Chapter 2. Since the GaAs substrates were oriented 2° off (001) towards [110], the x-ray peak position (ω) varied sinusoidally with speciman rotation angle (R) with a periodicity of 360°. In order to determine the real peak positions, rocking curves were obtained at two specimen rotation angles separated by 180° and the average of the peak positions from the two scans was taken as the true value of ω. HRXRD analysis was conducted on asymmetric (444) planes and the perpendicular and parallel lattice-mismatches were evaluated with respect to the GaAs substrate assuming tetragonal distortion.

An example of residual strain analysis concerning a 0.5μm thick $In_{0.14}Ga_{0.86}As$ layer follows. HRXRD rocking curves were obtained from the asymmetric (444) plane using the ω^- condition at +90° and -90° specimen rotation angles (see chapter 2) and these curves are shown in Figure 5-1. The ω^- peak position for the substrate and epilayer were determined from the two curves and were averaged to obtain the true ω^- ($\omega^- = \theta - \phi$) values of 16.2156° and 14.8361° for substrate and epilayer, respectively. A similar procedure was

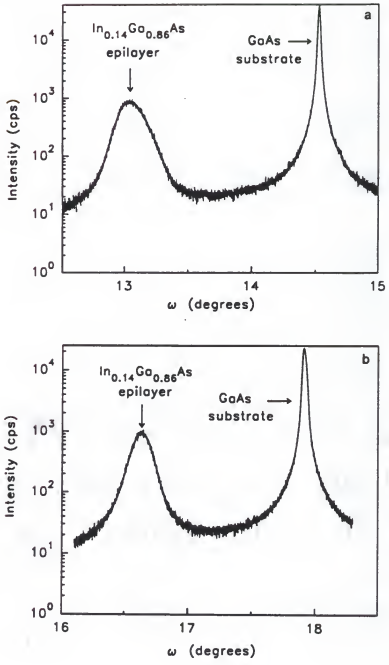

Figure 5-1. X-ray rocking curves obtained using the ω^- Bragg condition at (444) reflections.
a) -90° rotation angle and b) +90° rotation angle.

employed in the determination of true ω^+ ($\omega^+ = \theta + \phi$) values from the scans shown in Figure 5-2 which were found to be 125.5° and 124.3274°, respectively, for substrate and epilayer. The equations for ω^- and ω^+ were solved to obtain the values of θ and ϕ for substrate and epilayer, respectively. These values were used in the equations given in Chapter 2 to determine the perpendicular and in-plane or parallel lattice-mismatches between epilayer and substrate. For the example shown in Figures 5-1 and 5-2, the perpendicular and parallel mismatches were found to be 10,200ppm (1.02%) and 6500ppm (0.65%), respectively. The error in such calculations is about 5% of the mismatch value. The calculated perpendicular lattice-mismatch agreed with the lattice-mismatch determined using the (004) planes and hence the assumption of tetragonal distortion appeared to be valid.

The theoretical or relaxed lattice-mismatch is given by

$$\left(\frac{a_{epilayer} - a_{GaAs}}{a_{GaAs}}\right)_{relaxed} = \frac{(a_{InAs} - a_{GaAs})x}{a_{GaAs}}$$

where x is the $In_xGa_{1-x}As$ composition and a is the lattice parameter. The residual strain in the layer can be written as

$$\varepsilon_{\parallel} = \left[\left(\frac{\Delta a}{a_{GaAs}}\right)_{\parallel} - \left(\frac{\Delta a}{a_{GaAs}}\right)_{relaxed}\right] \frac{a_{GaAs}}{a_r}$$

where the parallel symbol denotes the in-plane mismatch that is experimentally determined using HRXRD and a_r is the fully relaxed lattice parameter of the epilayer. The equation is normalized to the lattice parameter at a particular $In_xGa_{1-x}As$ composition. For comparison of the relaxation between single layers of differing

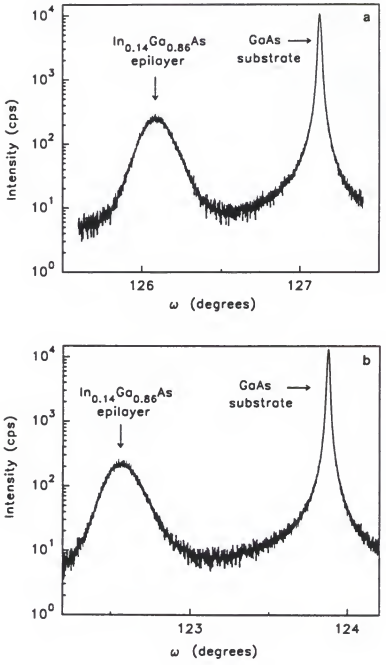

Figure 5-2. X-ray rocking curves obtained using the + Bragg condition at (444) reflections.
a) -90° rotation and b) +90° rotation.

compositions a "percentage relaxation" of the layer in the in-plane direction is defined as

$$\% \text{ relaxation} = \left\{ 1 - \frac{\left[\left(\frac{\Delta a}{a_{GaAs}}\right)_{\parallel} - \left(\frac{\Delta a}{a_{GaAs}}\right)_{relaxed}\right]}{\left(\frac{\Delta a}{a_{GaAs}}\right)_{relaxed}} \right\} \times 100$$

and the percent-relaxation is normalized to the fully relaxed lattice-mismatch strain. In order to obtain the relaxation in the perpendicular direction, the perpendicular lattice-mismatch is used instead of the in-plane mismatch in the equation given above.

$In_{0.14}Ga_{0.86}As$ layers were grown to various thicknesses and the extents of relaxation in the perpendicular and parallel directions were determined as a function of epilayer thickness (Figure 5-3). The plot in Figure 5-3 shows that strain relaxation in the perpendicular direction is complete at a thickness of 0.5μm. The strain in the perpendicular direction for layer thicknesses smaller than 0.5μm was found to be tensile in nature. Relaxation in the parallel or in-plane direction, however, was not complete even at a thickness of 2μm. Strain relaxation occurs rapidly up to a thickness of ~0.5μm, as evidenced by the steep slope in the percent relaxation versus thickness curve which suggests 66% strain relief at 0.5μm. As can be seen from Figure 5-3, relaxation becomes sluggish with further increase in layer thickness, showing only 9% further relaxation up to a thickness of 2μm.

$In_xGa_{1-x}As$ layers having compositions in the range, x=0.05-0.4, were grown to a constant thickness of 1μm. Also, three $In_xGa_{1-x}As$

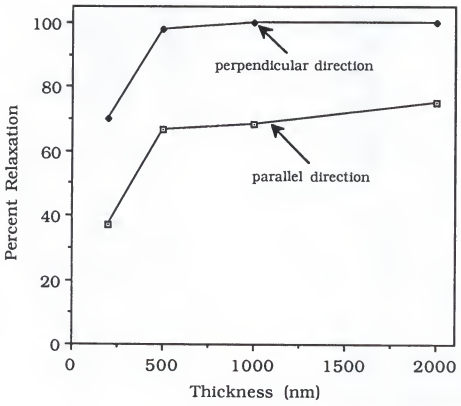

Figure 5-3. A plot of the percent relaxation in the perpendicular and parallel directions as a function of thickness in a $In_{0.14}Ga_{0.86}As/GaAs$ layer.

layers with x values of 0.14, 0.27 and 0.4, respectively, were grown to a thickness of 0.2μm to study the effect of composition on strain relaxation. HRXRD analysis performed on these layers showed that the extent of relaxation was almost a constant (70%) in 1μm thick $In_xGa_{1-x}As$ layers irrespective of composition (Figure 5-4). The thickness at which the relaxation rate (with respect to thickness) becomes slow might depend on the misfit strain which in turn is a function of epilayer composition. Data from the 0.2μm thick $In_xGa_{1-x}As$ layers suggests that in the $In_{0.14}Ga_{0.86}As$ layer (small misfit strain) only about 37% of the mismatch strain is relaxed whereas in $In_{0.27}Ga_{0.73}As$ and $In_{0.4}Ga_{0.6}As$ layers (large misfit strains) of the same thickness about 67% of the strain is relaxed (Figure 5-4). Thus one can conclude that $In_xGa_{1-x}As$ layers with larger mismatch strains reach the plateau, where strain relaxation is sluggish, at much smaller thicknesses compared to layers with smaller mismatch strains. Upon reaching this plateau, the extent of strain relaxation would appear to be a constant for any layer composition as evidenced by the data shown in Figure 5-4.

Currently published theories on strain relaxation [18,19,22] predict values of residual strain as a function of epilayer thickness. In order to compare theory with experimental data, a plot of the residual strain versus thickness for all $In_xGa_{1-x}As$ layer compositions studied in this work is shown in Figure 5-5. Strain relaxation theories by Matthews [3,4,18] and Tsao et al. [19] based on equilibrium force balance and plastic flow, respectively, suggest that residual strain is independent of $In_xGa_{1-x}As$ composition and only a function of epilayer

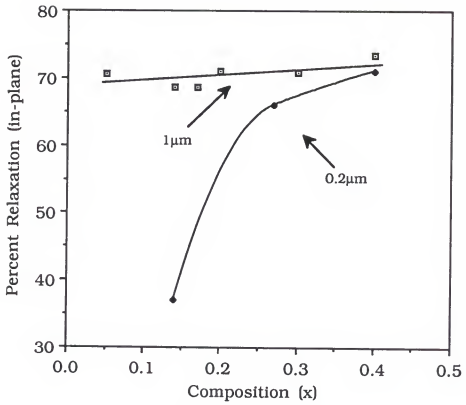

Figure 5-4. A plot of the in-plane relaxation as a function of $In_xGa_{1-x}As$ composition, x, at epilayer thicknesses of 0.2 and 1μm.

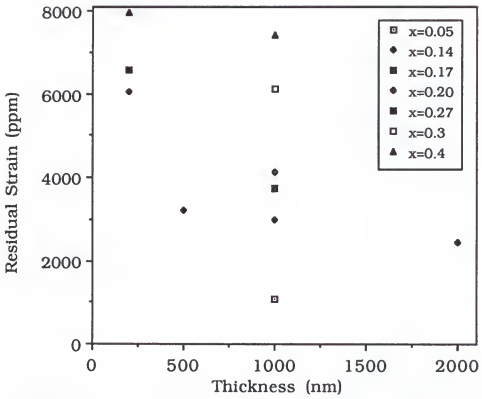

Figure 5-5. Residual strain data obtained for various $In_xGa_{1-x}As$ compositions and plotted as a function of thickness showing that the data is scattered and does not follow any obvious trend.

thickness. However, as can be seen from Figure 5-5, the residual strain is a strong function of $In_xGa_{1-x}As$ layer composition, ranging from 1000 to 8000ppm with increasing composition in the range x=0.05-0.4. Therefore, it can be concluded that these composition independent theories are invalid in the $In_xGa_{1-x}As/GaAs$ material system.

Maree et al. [22] proposed a strain relaxation theory based on the nucleation of surface half-loops and, as shown in Chapter 1, experimental data from various studies [9,22-24] on the $In_xGa_{1-x}As/GaAs$ system appear to fit the theoretical predictions within an error of about 2000ppm. However, for the composition range studied (x=0.07-0.25) such an error is significant. Even though Maree et al. [22] suggest that their theory is composition independent, they employ a critical half-loop radius, defined as that radius of a half-loop which maximizes the energy of the loop, which is a function of the critical thickness in their calculations. The critical thickness, in turn, is a function of $In_xGa_{1-x}As$ composition. The equation for residual strain as given by Maree et al. [22] is as follows:

$$\varepsilon = \sqrt{\frac{b}{240}\,\frac{1-\nu/2}{1+\nu}\,\frac{1}{h}\left(\ln\frac{4r_c}{b}-\frac{1}{2}\right)}$$

where r_c is the critical radius of the half-loop and h is the thickness of the epilayer. Maree et al. [22] state that the thickness of the layer must be maintained such that $h \geq r_c \sin\phi$ where ϕ is the angle between the glide-plane of a dislocation and the plane of the surface. It is well known that strain relaxation occurs when the thickness of the epilayer exceeds the critical thickness (h_c). Therefore, one can assume that

for the surface half-loop nucleation theory to hold true, $h_c=r_c\sin\phi$. Since the critical thickness decreases with increasing composition, r_c would also decrease with increasing composition since ϕ remains a constant for a specific crystal structure. Such a result, however, suggests that residual strain in the $In_xGa_{1-x}As$ layer would decrease with increasing composition (x) which is contrary to the experimental observations reported in this study (Figure 5-5). Thus, Maree et al.'s [22] surface half-loop nucleation theory cannot explain strain relaxation in the $In_xGa_{1-x}As/GaAs$ material system.

5.3 Strain Relaxation in Stacked $In_xGa_{1-x}As$ Multilayer Structures

A schematic of a multilayer structure is shown in Figure 5-6, in order to facilitate a description of the results obtained in this case. A stage number is assigned to each layer forming the stacked structure, the numbers increasing with increasing distance from the substrate. The thickness of each layer was 0.2μm unless otherwise specified. Separately grown multilayer structures comprising n stages, where n=1 to 8, were analysed by HRXRD and XTEM with the results obtained from analysis of each stage being used as the basis for the design of each subsequent stage.

Since, as discussed in the above section, strain relaxation is not complete particularly in the case of thin $In_xGa_{1-x}As$ epilayers, one can think of an unrelaxed $In_xGa_{1-x}As$ layer as having an "effective composition" which will always be less than the actual composition. In this work, such an "effective composition" (xn') for the $In_{xn}Ga_{1-xn}As$ layer, is defined as the composition corresponding to the in-plane

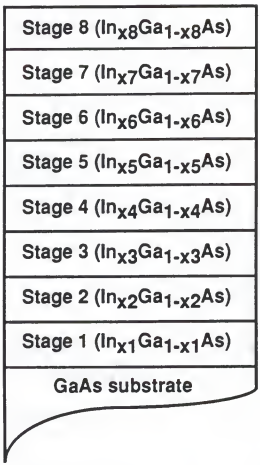

Figure 5-6. Schematic of the stacked $In_xGa_{1-x}As$ multilayer system grown by molecular beam epitaxy on GaAs. The schematic shows a total of eight stages (eight $In_xGa_{1-x}As$ layers), however, stacks with various numbers of stages were grown and analysed.

lattice parameter of the partially relaxed layer (accounting for strain) which is evaluated using Vergard's law as follows :

$$x_{n'} = \frac{(a_{n'} - a_{GaAs})}{(a_{InAs} - a_{GaAs})}$$

Furthermore, an "effective compositional difference" ($\Delta x'$) between two adjacent stages in the multilayer structure, for example stages n and (n+1), is defined as the difference between the relaxed composition, x(n+1), of the $(n+1)^{th}$ stage and the effective composition, xn', of the n^{th} stage.

In Chapter 3 the notion of a "critical composition" (x=0.18) for single $In_xGa_{1-x}As$ layers grown on GaAs was evoked. In this section this notion is extended to multilayer structures and a "critical compositional difference", Δx=0.18, is designated with respect to two adjacent layers in a stack.

Stage 1 of the multilayer structure comprised an $In_{0.14}Ga_{0.86}As$, i.e. x1=0.14, layer grown on GaAs. Since the epilayer composition is below the "critical composition" (x=0.18), the dislocations are confined to the heterointerface and the substrate as previously outlined in Chapter 3. Using HRXRD, the parallel lattice-mismatch between Stage 1 and the GaAs substrate was determined to be only 0.36% which is well below the theoretical (completely relaxed) lattice parameter mismatch (Table 5-1) of 1%, as evaluated assuming Vergard's law, and hence Stage 1 is only partially relaxed. The experimentally determined lattice parameter corresponds to an "effective" epilayer composition of x1'=0.05, compared to an actual composition of 0.14.

Table 5-1. HRXRD data from three separately grown structures consisting of one-, two- and three-stages, respectively, denoting the experimentally determined in-plane lattice-mismatch of the appropriate stages in each structure with respect to GaAs. The actual compositions of the three stages were x1=0.14, x2=0.22 and x3=0.3. All stages were 0.2μm thick. The relaxed lattice-mismatch of each stage with respect to GaAs is given in brackets below the corresponding stage number. The relaxed compositions of the top layers are denoted in brackets next to their effective compositions.

Structure #	Measured in-plane lattice-mismatch (%)			Effective composition of the top layer
	Stage 1 (1.0)	Stage 2 (1.58)	Stage 3 (2.15)	
1	0.36	-	-	0.05 (0.14)
2	0.80	1.0	-	0.14 (0.22)
3	0.83	1.24	1.42	0.20 (0.30)

Two separate structures consisting of $In_{x2}Ga_{1-x2}As$ (Stage 2) compositions of x2=0.22 and x2=0.27 were grown with Stage 1 in each case being x1=0.14 such that the effective compositional difference between the top layer and the underlying $In_{x1'}Ga_{1-x1'}As$ (effective composition) layer would be, in one case, smaller than the critical compositional difference (x2-x1'<0.18) and in the other case, greater than the critical compositional difference (x2-x1'>0.18). XTEM analysis of the structure containing the $In_{0.22}Ga_{0.78}As$ (Stage 2) epilayer showed dislocation evolution at the $In_{0.22}Ga_{0.78}As$/ $In_{0.14}Ga_{0.86}As$ (Stage2/Stage1) heterointerface and in the underlying $In_{0.14}Ga_{0.86}As$ layer (Figure 5-7a). Also, threading dislocations were not observed in the top $In_{0.22}Ga_{0.78}As$ layer. In contrast, XTEM analysis of the structure containing the $In_{0.27}Ga_{0.73}As$ (Stage 2) epilayer revealed threading dislocations in the top $In_{0.27}Ga_{0.73}As$ layer as well as dislocations in the $In_{0.14}Ga_{0.86}As$ (Stage 1) underlying layer (Figure 5-7b).

The above results can be explained as follows. If the effective compositional difference between the $In_xGa_{1-x}As$ layers in the two stages is below the critical compositional difference as is the case in the structure of Figure 5.7a, the surface image force, which is an inverse function of layer thickness, would not be significant enough to attract dislocations to the surface due to the larger critical thickness required to generate misfit dislocations. Also, if the yield strength of the top $In_{x2}Ga_{1-x2}As$ layer at its growth temperature is greater than that of the underlying $In_{x1}Ga_{1-x1}As$ layer, dislocation evolution would occur at the two heterointerfaces and in the underlying $In_{x1}Ga_{1-x1}As$

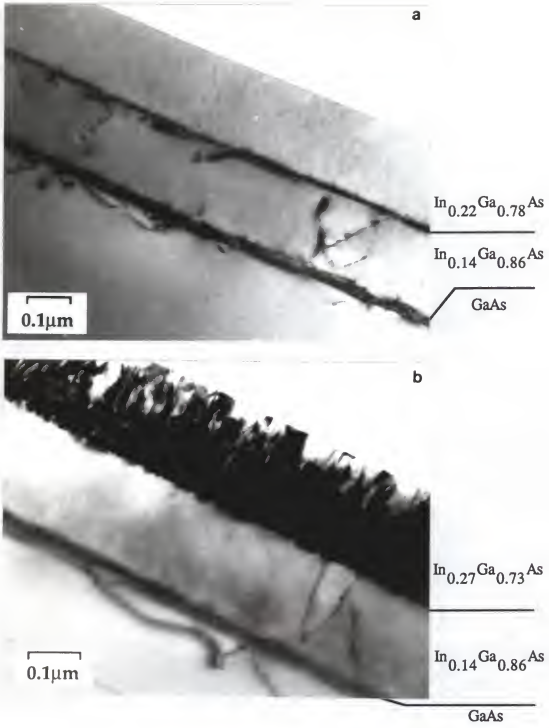

Figure 5-7. Cross-sectional transmission electron micrographs of two-stage structures.
a) Effective compositional difference smaller than the critical compositional difference and b) Effective compositional difference greater than the critical compositional difference.

layer and the GaAs substrate as is observed in the micrograph. However, if the effective compositional difference between the $In_xGa_{1-x}As$ layers is greater than the critical compositional difference, as is the case in the structure of Figure 5-7b, the surface image force will be comparable to the additional forces acting on a dislocation at the $In_{x2}Ga_{1-x2}As/In_{x1}Ga_{1-x1}As$ heterointerface since the critical thickness in this case will be small. Thus, the dislocations can traverse to the surface even though the yield strength of the top layer is greater than that of the underlying layer. The composition of x2=0.22 was used for the second stage in all subsequent multilayer structures since no threading dislocations were observed in the structure consisting of a Stage 2 having this composition.

HRXRD analysis indicated that the effective composition (taking into account partial strain relaxation) of the selected Stage 2 $In_{x2}Ga_{1-x2}As$ layer (x2=0.22) is x2'=0.14 (Table 5-1). Therefore, an $In_{x3}Ga_{1-x3}As$ composition of x3=0.3 was chosen for Stage 3 of the stacked structure since x3-x2'<0.18. By the same reasoning, a Stage 4 composition of x4=0.35 was selected since, as shown in Table 5-1, the effective composition of Stage 3 (x3=0.3) was x3'=0.2 giving again an effective compositional difference <0.18 at the Stage 3/Stage 4 heterointerface. XTEM analysis of three-stage and four-stage structures showed a lack of threading dislocations in the top $In_xGa_{1-x}As$ layer of each stack as illustrated in Figures 5-8a and 5-8b. Strain relief occurs by the formation of dislocations at the heterointerfaces and in the underlying layers (Stages 1-3). Etch pit analysis of the $In_{0.35}Ga_{0.65}As$ top layer which in this case was 1μm

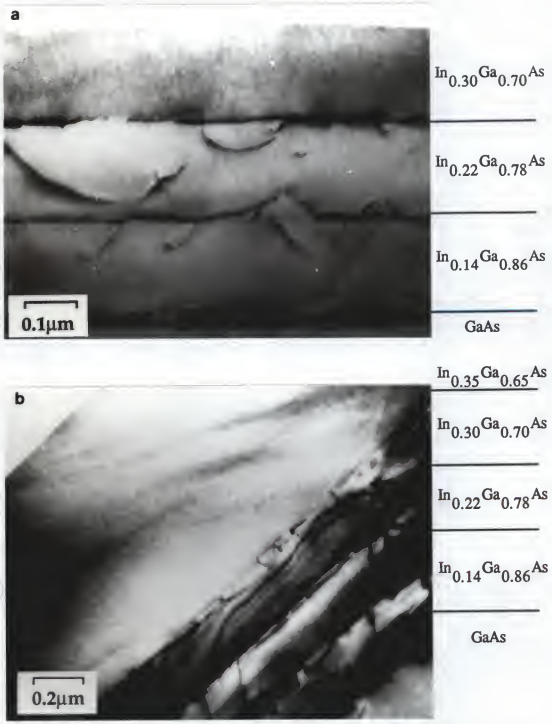

Figure 5.8: Cross-sectional transmission electron micrographs of showing dislocations in underlying layers and a noticable absence of dislocations in the top $In_xGa_{1-x}As$ layer of multilayer structures.
a) three-stage structure and b) four-stage structure.

thick revealed a threading dislocation density of only 1-2x$10^3/cm^2$ in this material (Figure 5-9).

HRXRD data obtained from one-, two- and three-stage structures is detailed in Table 5-1. As can be seen from the table, in each case the top layer is only partially relaxed. Also, strains in the underlying $In_xGa_{1-x}As$ layers approach their theoretical values with increasing number of stages suggesting that underlying layers continue to undergo strain relief by the generation of dislocations upon growth of additional stages. It is also noted that provided the thickness of the top layer and the effective compositional difference with respect to the underlying layer is maintained a constant, the extent of in-plane relaxation of the top $In_xGa_{1-x}As$ layer with respect to its underlying layer is almost a constant as evidenced by the nearly constant difference between the actual composition and the effective composition of the top layer following each stage of growth. This observation seems to suggest a monotonic increase in yield strength at the growth temperature for $In_xGa_{1-x}As$ with increasing values of x at least up to x=0.3 since, the extent of relaxation is a direct function of yield strength.

Three multilayer structures consisting of 5, 6 and 7 stages, respectively, were grown with compositions of x5=0.4, x6=0.45 and x7=0.48 above Stage 4 (x4=0.35,0.2μm) such that the effective compositional difference between the top two stages in each of the three structures was well below the critical compositional difference. Stages 1-4 were maintained identical in each case. The composition of the seventh stage was chosen to be x7=0.48 since it is a composition of interest for potential device operation at 1.55μm and

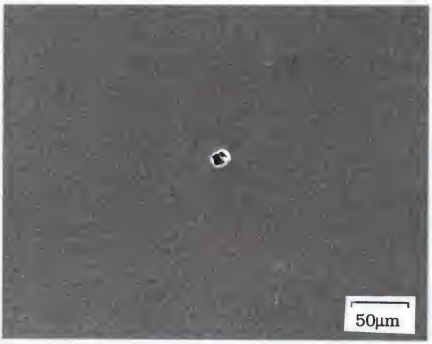

Figure 5-9. Scanning electron micrograph showing an etch-pit in the top $In_{0.35}Ga_{0.65}As$ layer of a four-stage heterostructure. Dislocation density was calculated to be ~$10^3/cm^2$.

the thickness of this stage was selected as 1μm to enable etch pit analysis of the layer. XTEM analysis of the multilayer structures showed that strain relief continues to occur by the generation of dislocations at the heterointerfaces and in the underlying stages as shown in Figures 5-10a and 5-10b which show the structures containing six and seven stages, respectively. Etch pit analysis of the $In_{0.48}Ga_{0.52}As$ layer revealed a threading dislocation density of only $5\text{-}6x10^3/cm^2$ (Figure 5-11). These observations seem to indicate that the yield strength of the top layer at the growth temperature is larger than that of the underlying layer at each stage which leads to dislocation formation (yielding) always in the underlying layers. It is to be noted that the observed dislocation density is three orders of magnitude smaller than that obtained by using the multi-stage strain relief buffer described in the previous chapter even though the top layer composition (x=0.48) employed in this heterostructure is larger than that in the top layer (x=0.4) of the buffer system involving SLSs.

Finally, a heterostructure consisting of 8 stages was grown in which stages 7 and 8 having compositions, x7=0.5 and x8=0.53, respectively, were grown above Stage 6 (x6=0.45). Stages 1-5 were identical to those involved in the structure consisting of five stages. XTEM analysis of the eight stage structure revealed threading dislocations in the $In_{0.53}Ga_{0.47}As$ top layer as shown in Figures 5-12a and 5-12b. Dislocations, however, were not observed in the underlying $In_{0.5}Ga_{0.5}As$ (Stage 7) layer. Since the effective compositional difference between the top two layers is below the critical compositional difference, the presence of dislocations in the top layer and not its underlying layer is explained if the yield strength

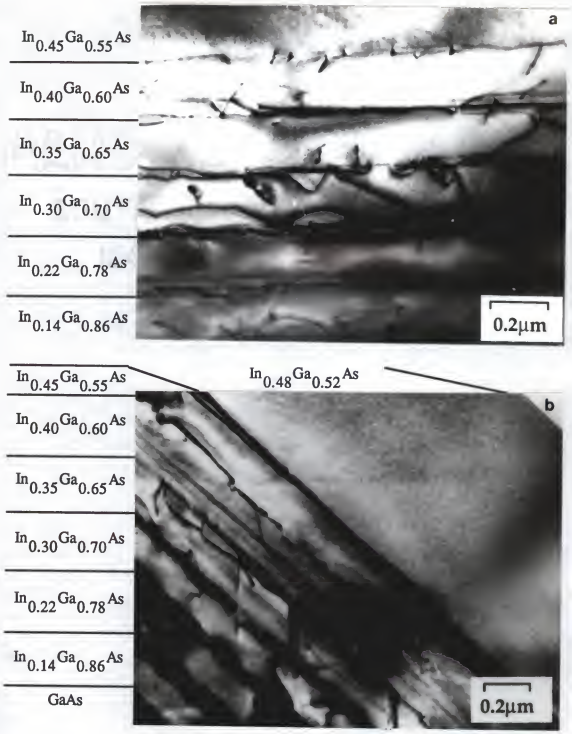

Figure 5-10. Cross-sectional transmission electron micrographs of multilayer structures showing a lack of threading dislocations in the top layer of each structure and extensive dislocation evolution in the underlying layers. a) six-stage structure and b) seven-stage structure.

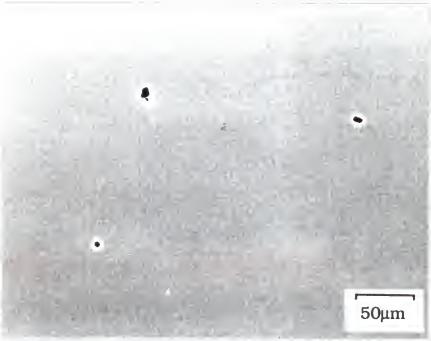

Figure 5-11. Scanning electron micrograph showing etch-pits in the top $In_{0.48}Ga_{0.52}As$ layer of a seven-stage structure. Dislocation density was calculated to be $5\text{-}6x10^3/cm^2$ in this material

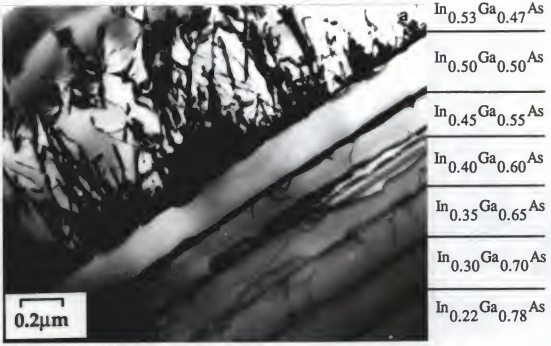

Figure 5-12. Cross-sectional transmission electron micrographs of an eight-stage structure.
a) Showing almost the whole structure with the exception of the GaAs substrate and the $In_{0.14}Ga_{0.86}As$ layer;

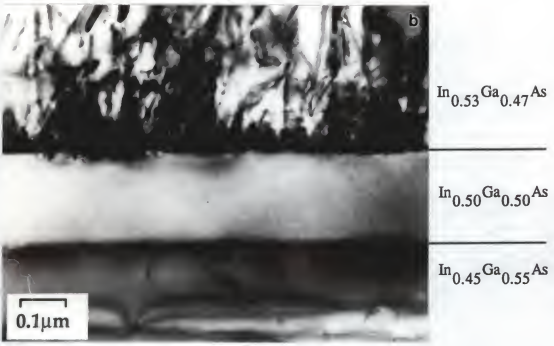

Figure 5-12--continued

b) An $In_{0.5}Ga_{0.5}As$ (Stage 7) layer sandwiched between the $In_{0.53}Ga_{0.47}As$ (Stage 8) and $In_{0.45}Ga_{0.55}As$ (Stage 6) layers. The micrograph shows an apparant lack of dislocations in the $In_{0.5}Ga_{0.5}As$ layer and threading dislocations in the $In_{0.53}Ga_{0.47}As$ layer. The critical compositional difference was not exceeded at any of the heterointerfaces, however, the yield strength of $In_{0.53}Ga_{0.47}As$ at the growth temperature would appear to be smaller than that of $In_{0.5}Ga_{0.5}As$, resulting in dislocation evolution in the $In_{0.53}Ga_{0.47}As$ material.

at the growth temperature of $In_{0.53}Ga_{0.47}As$ is smaller than that of $In_{0.5}Ga_{0.5}As$. The absence of dislocations in the $In_{0.5}Ga_{0.5}As$ layer suggests that its yield strength is greater than that of the underlying $In_{0.45}Ga_{0.55}As$ layer.

Studies reported in the literature [65,66] on the high temperature mechanical properties of InAs and GaAs using compression tests have shown that InAs has a lower yield strength than GaAs at an elevated temperature (540°C). Combining the dislocation evolution information obtained in this work and available data on the high temperature yield strengths for binary InAs and GaAs, one can sketch the yield strength (in arbitrary units) of $In_xGa_{1-x}As$ as a function of In content with respect to the particular temperatures employed for alloy growth as shown in Figure 5-13. For the growth temperatures employed in this study, a peak in the yield strength would seem to occur at an In content of x=0.5. Therefore, for x<0.5, one can use the notion of "critical compositional difference" to obtain low-dislocation density $In_xGa_{1-x}As$ alloys grown on GaAs, since strain relief occurs by the generation of dislocations in the softer (lower yield strength) material i.e. the underlying layer in the structure, and, since below the critical compositional difference the surface image force is not large enough to influence the dislocations at the heterointerface.

In this study, all of the $In_xGa_{1-x}As$ sacrificial layers in the multilayer system were grown to a thickness of 0.2μm. However, based on the residual strain studies performed on single $In_xGa_{1-x}As$ layers grown on GaAs detailed in the previous section, it should be possible to employ fewer stages in the multi-stage system in order to

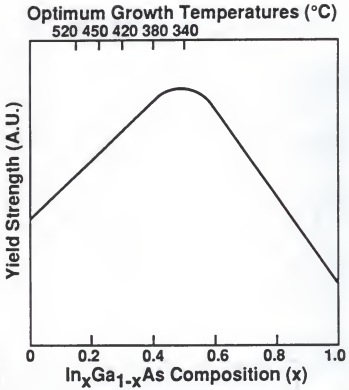

Figure 5-13. A conceptual plot of the yield strength at the growth temperature versus $In_xGa_{1-x}As$ composition based on indirect evidence from dislocation evolution and strain relief studies (see text). The $In_xGa_{1-x}As$ layers employed in this study and their corresponding growth temperatures are as follows: x=0.14, 520°C; x=0.22, 450°C; x=0.3, 420°C; x=0.35, 400°C; x=0.4, 380°C; x=0.45, 360°C; x=0.48, 350°C; x=0.5, 340°C and x=0.53, 330°C.

achieve a particular $In_xGa_{1-x}As$ composition by growing thicker sacrificial layers than were grown in this study.

CHAPTER 6
CONCLUSIONS AND RECOMMENDATIONS

Several conclusions can be drawn from the work described in this dissertation which are as follows:

a) A "critical composition" of $x \approx 0.18$ exists for the $In_xGa_{1-x}As$/ GaAs heteroepitaxial system above which threading dislocations propagate into the $In_xGa_{1-x}As$ epilayer and, in general, dislocation evolution in the $In_xGa_{1-x}As$/GaAs system as a function of composition can be explained employing a force balance model which includes a surface image force term.

b) $In_xGa_{1-x}As$ layers with relatively low-dislocation densities ($\approx 10^6/cm^2$) can be grown indirectly on GaAs up to a composition of $x \approx 0.4$ using multistage buffer structures consisting of conventional dislocation blockers, i.e. strained-layer superlattices. The inability of such multistage buffer structures to reduce the dislocation density in $In_xGa_{1-x}As$ layers having $x > 0.4$ appears to be due to dislocation nucleation and evolution within the SLSs comprising the buffer.

c) Strain relaxation in $In_xGa_{1-x}As$/GaAs layers is complete in the perpendicular (growth) direction at relatively small layer thicknesses (~0.5μm), however, a finite (~25%) residual strain exists in the in-plane direction even for relatively thick layers. Residual strain in the $In_xGa_{1-x}As$ layers is strongly dependent on both the layer thickness

and composition, decreasing with increasing thickness and increasing with increasing composition.

d) Extremely low-dislocation density ($<10^4/cm^2$) $In_xGa_{1-x}As$ layers can be grown up to an x value of ~0.5 indirectly on GaAs by use of multilayer epitaxial structures that do not involve conventional buffers. Such structures are designed such that the "effective compositional difference" (accounting for partial relaxation) between successive $In_xGa_{1-x}As$ layers in the stack is below a "critical compositional difference" of $x \approx 0.18$.

e) A monotonic increase in the elevated temperature yield strength of $In_xGa_{1-x}As$ as a function of composition is suggested, based on indirect evidence, for x values in the range, 0 to 0.5, while the alloy yield strength is suggested to decrease with increasing composition for x values >0.5 for the growth temperatures employed in this study.

The above conclusions suggest several possibilities for future research, both fundamental and applied, in the field of compound semiconductor heteroepitaxy. On a fundamental note, the present work has highlighted the need for data on the elevated temperature mechanical properties of compound semiconductors, particularly ternary and quarternary alloys. Such data could indicate the possibility of growing device quality alloys in other lattice-mismatched systems assuming that they would behave in a manner similar to that displayed by the $In_xGa_{1-x}As/GaAs$ system, i.e., the alloy would have to be harder at the appropriate growth temperature.

On the applied research front, dislocation-sensitive devices such as light emitting diodes and diode lasers could be designed based on large In content, low-dislocation density $In_xGa_{1-x}As$ material. The

testing of such devices should further demonstrate the high-quality nature of the $In_xGa_{1-x}As$ material which has been achieved as a result of the fundamental work described in this dissertation. A more far reaching research area would be the design of monolithically integrated photonic devices operating at 1.3 and 1.55μm with GaAs ICs.

REFERENCES

1. S. Adachi, J. Appl. Phys., **53**, 8775 (1982).

2. J.H. Van der Merwe, J. Appl. Phys., **34**, 123 (1962).

3. J.W. Matthews, S. Mader and T.B. Light, J. Appl. Phys., **41**, 3800 (1970).

4. J.W. Matthews, A.E. Blakeslee and S. Mader, Thin Solid Films, **33**, 253 (1976).

5. J.W. Matthews in "Dislocations in Solids", Ed. F.R.N. Nabarro, North Holland Publishing Company, London (1979).

6. R. People and J.C. Bean, Appl. Phys. Lett., **47**, 322 (1985).

7. R. People and J.C. Bean, Appl. Phys. Lett., **49**, 229 (1986).

8. H. Nakao and T. Yao, Jap. J. Appl. Phys., **28**, 352 (1989).

9. P.J. Orders and B.F. Usher, Appl. Phys. Lett., **50**, 980 (1987).

10. I.J. Fritz, P.L. Gourley and L.R. Dawson, Appl. Phys. Lett., **51**, 1004 (1987).

11. G.L. Price, Appl. Phys. Lett., **53**, 1288 (1988).

12. P. Berger, K. Chang, P. Bhattacharya, J. Singh and K.K. Bajaj, Appl. Phys. Lett., **53**, 684 (1988).

13. H. Munekata, L.L. Chang, S.C. Woronick and Y.H. Yao, J. Cryst. Growth, **81**, 237 (1987).

14. G.L. Price, Phys. Rev. Lett., **66**, 469 (1991).

15. P.R. Berger, K. Chang, P.K. Bhattacharya and J. Singh, J. Vac. Sci. Technol. B, **5**, 1162 (1987).

16. B. F. Lewis, T.C. Lee, F.J. Grunthaner, A. Madhukar, R. Fernandez and J. Maserjian, J. Vac. Sci. Technol. B, **2**, 419 (1984).

17. G.J. Whaley and P.I. Cohen, J. Vac. Sci. Technol. B, **6**, 625 (1988).

18. J.W. Matthews and A.E. Blakeslee, J. Cryst. Growth, **27**, 118 (1974).

19. J.Y. Tsao, B.W. Dodson, S.T. Picraux and D.M. Cornelison, Phys. Rev. Lett., **59**, 2455 (1987).

20. B.W. Dodson and J.Y. Tsao, Appl. Phys. Lett., **51**, 1325 (1987).

21. B.W. Dodson and J.Y. Tsao, Appl. Phys. Lett., **52**, 852 (1988).

22. P.M.J. Maree, J.C. Barbour and J.C. van der Veen, J. Appl. Phys., **62**, 4413 (1987).

23. A.V. Drigo, Y. Aydinli, A. Carnera, F. Genova, C. Rigo, C. Ferrari, P. Franzosi and G. Salviati, J. Appl. phys., **66**, 1975 (1989).

24. K. Kamigaki, H. Sakashita, H. Kato, M. Nakayama, N. Sano and H. Terauchi, Appl. Phys. Lett., **49**, 1071 (1986).

25. B.W. Dodson, Appl. Phys. Lett., **53**, 394 (1988).

26. J.P. Hirth and J. Lothe, "Theory of Dislocations", McGraw-Hill Publishers, New York (1968).

27. B.W. Dodson, Phys. Rev. B, **35**, 5558 (1987).

28. E.A. Fitzgerald, D.G. Ast, P.D. Kirchner, G.D. Pettit and J.M. Woodall, J. Appl. Phys., **63**, 693 (1988).

29. E.A. Fitzgerald, D.G. Ast, Y. Ashizawa, S.Akbar and L.F. Eastman, J. Appl. Phys., **64**, 2473 (1988).

30. C. Herbeaux, J. Di Persio and A. Lefebvre, Appl. Phys. Lett., **54**, 1994 (1988).

31. J. Kleiman and R.M. Park, J. Appl. Phys., **61**, 2067 (1987).

32. H.L. Tsai and Y.C. Kao, J. Appl. Phys., **67**, 2862 (1990).

33. K.H. Chang, P.K. Bhattacharya and R. Gibala, J. Appl. Phys., **66**, 2993 (1989).

34. K.H. Chang, P.K. Bhattacharya and R. Gibala, J. Appl. Phys., **65**, 3391 (1989).

35. M. Tabuchi, S. Noda and A. Sasaki, J. Cryst. Growth, **99**, 315 (1990).

36. S. Guha, A. Madhukar and K.C. Rajkumar, Appl. Phys. Lett., **57**, 2110 (1990).

37. C.M.Serrano and C.A. Chang, Appl. Phys. Lett., **39**, 808 (1981).

38. Y.G. Chai and R. Chow, J. Appl. Phys., **53**, 1229 (1982).

39. C.A. Chang and C.M. Serrano, Appl. Phys. Lett., **37**, 538 (1980).

40. M. Ilegems in "The Technology and Physics of Molecular Beam Epitaxy", Ed. E.H.C. Parker, McGraw Hill Publishers, New York (1985).

41. G.P. Watson, D.G. Ast, T.J. Anderson, Y. Hayakawa and B. Pathangey, J. Electron. Mater., **20**, 703 (1991).

42. G.P. Watson, D.G. Ast, T.J. Anderson and Y. Hayakawa, Mater. Res. Soc. Extended Abstract (EA-21), Materials Research Society, 267 (1990).

43. N.A. El-Masry, J.C. Tarn and N.H. Karam, J. Appl. Phys., **64**, 3672 (1988).

44. K. Rajan, R. Devine, W.T. Moore and P. Maigne, J. Appl. Phys, **62**, 1713 (1987).

45. A. Lefebvre, C. Herbeaux and J. Di Persio, Phil. Mag. A, **63**, 471 (1991).

46. P. Ribas, Ph. D. dissertation, University of Florida (1990).

47. F. Riesz, K. Lischka, K. Rakennus, T. Hakkrainen and A. Pesek, J. Cryst. Growth, **114**, 127 (1991).

48. F. Riesz, K. Lischka, K. Rakennus, T. Hakkrainen, A. Pesek and E. Koppensteiner, to be published (1992).

49. P. Auvray, M. Baudet and A. Ragreny, J. Cryst. Growth, **95**, 228 (1989).

50. A. Pesek, K. Hingerl, F. Rieszc and K. Lischka, Semicond. Sci. Technol., **6**, 705 (1991).

51. J. Kleiman, R.M. Park, H.A. Mar, J. Appl. Phys., **64**, 1201 (1988).

52. R.M. Park, J. Kleiman and H.A. Mar, Proceedings of Society of Photo-optical Instrumentation Engineers, **796**, 86 (1987).

53. W.J. Bartels, J. Vac. Sci. Technol. B, **1**, 338 (1983).

54. W.J. Bartels and W. Nijman, J. Cryst. Growth, **44**, 518 (1978).

55. M.G. Tabache, E.D. Bourret and A.G. Elliot, Appl. Phys. Lett., **49**, 289 (1986).

56. E.D. Bourret, M.G. Tabache and A.G. Elliot, Appl. Phys. Lett., **50**, 1373 (1987).

57. E.D. Bourret, M.G. Tabache, J.W. Beeman, A.G. Elliot and M. Scott, J. Cryst. Growth, **85**, 275 (1987).

58. A. Djemel and J. Castaing, Europhys. Lett., **2**, 611 (1986).

59. H. Ehrenreich and J.P. Hirth, Appl. Phys. Lett., **46**, 668 (1985).

60. R.J. Arsenault in "Plastic Deformation of Materials", Treatise on Materials Science and Technology, Vol. 6, Ed. R.J. Arsenault, Academic Press, New York (1975).

61. J.C. Mikkelsen, Jr. and J.B. Boyce, Phys. Rev. B, **28**, 7130 (1983).

62. S. Guruswamy, J.P. Hirth and K.T. Faber, J. Appl. Phys., **60**, 4136 (1986).

63. J.P. Hirth and J. Lothe, "Theory of Dislocations", Wiley Publishers, New York (1982).

64. Y.C. Tzeng, S.S. Li, Y.W. Lin, P. Ribas and R.M. Park, Appl. Phys. Lett., **58**, 2396 (1991).

65. A.Zozime and J.Castaing, Inst. Phys. Conf. Ser. No 104, Int. Symp. on "Structural Properties of Dislocations in Semiconductors", Oxford (1989).

66. H.Gottschalk, G.Patzer and H.Alexander, Phys. Stat. Sol. A, **45**, 207 (1978).

BIOGRAPHICAL SKETCH

Viswanath Krishnamoorthy was born on October 26, 1965 in Trichy, India. He attended schools in Bombay and Salem, India, and Nairobi, Kenya, and graduated from high school at Padma Seshadri High School, Madras, India, in 1982. He then enrolled at the Indian Institute of Technology at Madras and graduated with a Bachelor of Technology degree (Metallurgy) in 1986. He proceeded to graduate school at the University of Florida (Department of Materials Science and Engineering) and, after completing his master's research, has been working towards his doctoral degree since September 1989. He formally obtained his Master of Science degree in 1991.

I certify that I have read this study and that in my opinion it conforms to acceptable standards of scholarly presentation and is fully adequate, in scope and quality, as a dissertation for the degree of Doctor of Philosophy.

Robert M. Park, Chairman
Associate Professor of Materials Science and Engineering

I certify that I have read this study and that in my opinion it conforms to acceptable standards of scholarly presentation and is fully adequate, in scope and quality, as a dissertation for the degree of Doctor of Philosophy.

Robert T. DeHoff
Professor of Materials Science and Engineering

I certify that I have read this study and that in my opinion it conforms to acceptable standards of scholarly presentation and is fully adequate, in scope and quality, as a dissertation for the degree of Doctor of Philosophy.

Paul H. Holloway
Professor of Materials Science and Engineering

I certify that I have read this study and that in my opinion it conforms to acceptable standards of scholarly presentation and is fully adequate, in scope and quality, as a dissertation for the degree of Doctor of Philosophy.

Kevin S. Jones
Assistant Professor of Materials Science and Engineering

I certify that I have read this study and that in my opinion it conforms to acceptable standards of scholarly presentation and is fully adequate, in scope and quality, as a dissertation for the degree of Doctor of Philosophy.

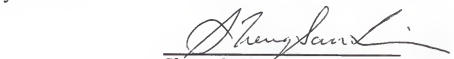

Sheng S. Li
Professor of Electrical Engineering

This dissertation was submitted to the Graduate Faculty of the College of Engineering and to the Graduate School and was accepted as partial fulfillment of the requirements for the degree of Doctor of Philosophy.

August 1992

Winfred M. Phillips
Dean, College of Engineering

Madelyn M. Lockhart
Dean, Graduate School